



# Filamented ion tail structures at Titan: A hybrid simulation study



Moritz Feyerabend<sup>a,b,\*</sup>, Sven Simon<sup>b</sup>, Uwe Motschmann<sup>c,d</sup>, Lucas Liuzzo<sup>b</sup>

<sup>a</sup> Institute of Geophysics and Meteorology, University of Cologne, Cologne, Germany

<sup>b</sup> School of Earth and Atmospheric Sciences, Georgia Institute of Technology, Atlanta, USA

<sup>c</sup> Institute for Theoretical Physics, University of Braunschweig, Braunschweig, Germany

<sup>d</sup> Institute for Planetary Research, German Aerospace Center, Berlin, Germany

## ARTICLE INFO

### Article history:

Received 5 May 2015

Received in revised form

20 July 2015

Accepted 23 July 2015

Available online 15 August 2015

### Keywords:

Titan

Cassini

Moon–magnetosphere interactions

Hybrid plasma simulation

## ABSTRACT

This study investigates the processes that lead to the detection of split signatures in ion density during several crossings of the Cassini spacecraft through Titan's mid-range plasma tail (T9, T63, and T75). During each of these flybys, the Cassini Plasma Spectrometer detected Titan's ionospheric ion population twice; i.e., the spacecraft passed through two spatially separated regions where cold ions were detected, with the regions also being dominated by ions of different masses in the case of T9. Whether this filamented tail structure is an omnipresent feature of Titan's plasma interaction or a result of non-stationary upstream conditions during specific flybys is still unclear. To explain these features, we apply the hybrid simulation code AIKEF (kinetic ions and fluid electrons). Our model includes chemical reactions as well as a realistic photoionization model for a sophisticated description of the ionospheric composition of Titan. Our simulations show that the filamentation of Titan's tail is indeed a common feature of the moon's plasma interaction. Light ionospheric species escape along draped magnetic field lines to form a parabolically shaped filament structure, which is mainly seen in planes that contain the upstream magnetospheric magnetic field and the upstream flow direction. In addition, transport of ions of all species from the ramside towards downstream produces a cone structure behind Titan, with a region of decreased density inside and filaments of 1–2  $R_T$  ( $R_T=2575$  km) thickness and enhanced density at the surface of the cone. Spacecraft trajectories that penetrate these structures allow for the detection of split signatures in the tail. The orientation of the upstream magnetic field and plasma flow as well as local time effects (i.e., Titan's orbital position) influence the location of the filaments in the tail and can also cause asymmetries in their sizes and densities. The detection of the split signatures along a spacecraft trajectory may therefore be made possible or completely prevented by moving the narrow filaments in or out of the way of the spacecraft. Our results imply that the detections of split signatures during T9, T63 and T75 are consistent by Cassini penetrating through parts of these filament structures.

© 2015 Elsevier Ltd. All rights reserved.

## 1. Introduction

Titan (radius  $R_T=2575$  km) is the largest moon of Saturn and possesses a dense neutral atmosphere, consisting mainly of molecular nitrogen. The ionosphere formed mainly by photoionization and, to a minor degree, electron impact (e.g., Coates et al., 2011; Galand et al., 2014) interacts with Saturn's impinging magnetospheric plasma, generating an induced magnetosphere around Titan: the magnetic field drapes around the obstacle and the plasma becomes mass-loaded by picking up new ions from Titan's ionosphere. The gyro radii of the pickup ions are of the same order as Titan's radius, producing an asymmetric tail downstream (e.g.,

Bertucci et al., 2011; Wahlund et al., 2014). Throughout the upper atmosphere, rich neutral and ion–neutral chemistry produce a complex admixture of neutral and charged species (e.g., Vuitton et al., 2007, 2014; Krasnopolsky, 2009).

Since its arrival at Saturn in 2004, the Cassini spacecraft has performed more than 100 flybys of Titan. Most of these flybys were aimed to pass Titan at low altitudes within 1  $R_T$  to study its ionospheric structure. The number of flybys which actually passed through Titan's tail, i.e., the population of pickup ions and/or magnetic wake downstream of Titan, with a closest approach altitude ( $C/A$ ) larger than 1  $R_T$  is much smaller. Simon et al. (2014) identified 19 encounters that are potentially suitable to study Titan's plasma tail at intermediate altitudes between 1  $R_T$  and 5  $R_T$ .

One interesting finding of the mid-range tail flybys were the so-called 'split signatures' (Coates et al., 2007b; Modolo et al., 2007b), i.e., two spatially separated regions populated by cold pickup ions observed during the T9 ( $C/A$  at 4  $R_T$  on 26 December

\* Corresponding author at: Institute of Geophysics and Meteorology, University of Cologne, Cologne, Germany.

E-mail address: [feyerabend@geo.uni-koeln.de](mailto:feyerabend@geo.uni-koeln.de) (M. Feyerabend).

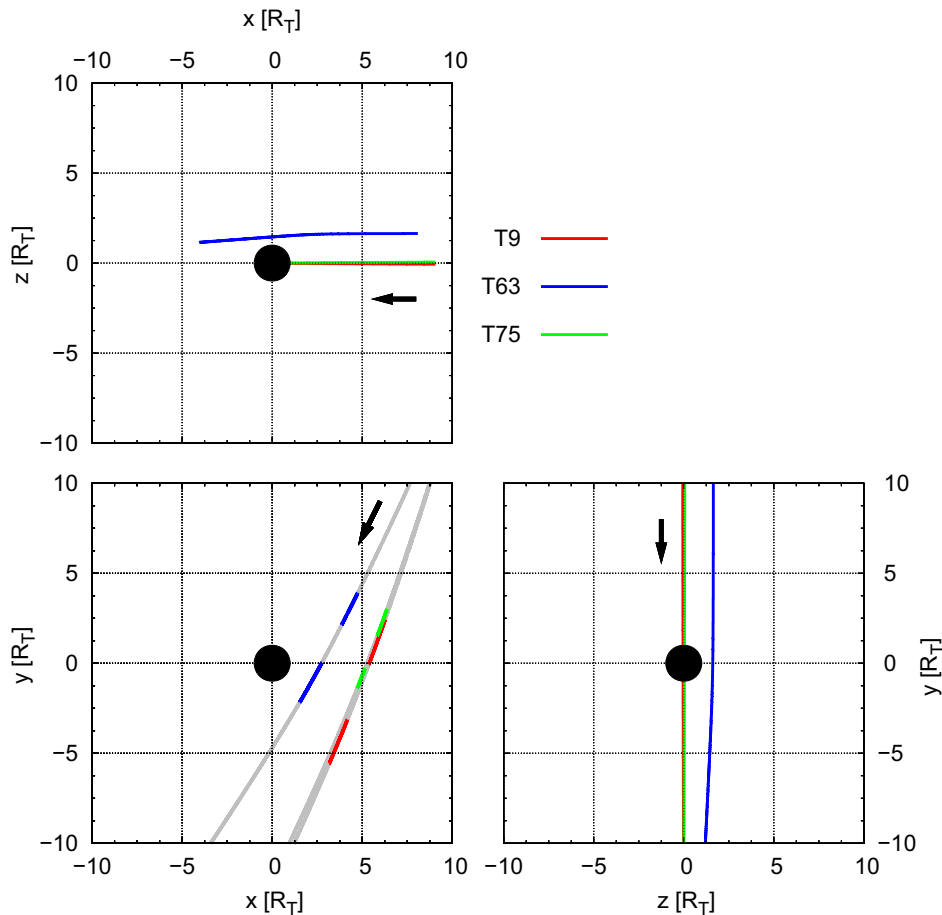


**Fig. 1.** Projections of the T9, T63 and T75 flyby trajectories onto the planes of the TIIS coordinate system. The colored intervals along the trajectories in the  $xy$  plane indicate the locations of the split signatures according to Coates et al. (2012). T9 and T75 occurred in Titan's equatorial plane, with nearly identical trajectories. T63 took place slightly north of Titan's equatorial plane. The flyby direction was the same for all encounters, indicated by the black arrows. (For interpretation of the references to color in this figure caption, the reader is referred to the web version of this paper.)

2005), T63 ( $C/A$  at  $1.9 R_T$  on 12 December 2009) and T75 ( $C/A$  at  $3.9 R_T$  on 19 April 2011) encounters. The trajectories of these flybys, with indications of the location of the split signatures, are shown in Fig. 1. The underlying coordinate system is the Titan Interaction System TIIS (Neubauer et al., 2006), where the  $x$ -axis is aligned with the corotation direction, the  $y$ -axis points towards Saturn and  $z$  completes the right-handed system, pointing northward. Under ideal conditions (incident flow  $\underline{u}_0$  aligned with the  $x$ -axis, ambient magnetic field quasi-dipolar and thus,  $\underline{B}_0$  anti-parallel to the  $z$ -axis) the undisturbed convective electric field  $\underline{E}_0 = -\underline{u}_0 \times \underline{B}_0$  would point in the  $-y$  direction.

Ion and electron spectra presented for T9 by Coates et al. (2007b), Szego et al. (2007) and Modolo et al. (2007b) showed the detection of cold ions and electrons of ionospheric origin in two spatially separated segments along the T9 trajectory (see Fig. 1). The ion compositions differed as well between the two segments with heavy ions (mass-to-charge ratio  $m/q=16$  and  $32$ ) dominating during the first segment and light ions (mass-to-charge ratio  $m/q=1$  and  $2$ ) dominating during the second segment (Coates et al., 2007b; Szego et al., 2007).

Szego et al. (2007) suggested that the second event was part of the distant pick-up tail of Titan and that during the first event ions were escaping along magnetic field lines due to the specific magnetic background geometry. Coates et al. (2007b) identified ionospheric particles in both events and suggested that the source of the ions in the second event was located on the nightside of Titan and at higher altitudes. Sittler et al. (2010) explained the second event as light ions that were picked up by draped field lines near the induced

magnetopause boundary. Similar split signatures have also been reported for the T63 and T75 encounters by Coates et al. (2012). However, for both of these flybys the individual filaments of the split tail contained an admixture of heavy ( $m/q=16$  and  $28$ ) and light ( $m/q=1$  and  $2$ ) ions, in contrast to T9. The authors also used Cassini Plasma Spectrometer (CAPS) data to constrain plasma escape rates for each flyby and concluded that Titan's ionosphere loses about 7 tonnes of mass per Earth day.

Magnetic field observations from the T9 encounter (Bertucci et al., 2007) showed that Titan was located below Saturn's magnetodisk, i.e., the magnetic field possessed significant components oriented towards Saturn and along the corotational flow direction (see also Bertucci et al., 2009). By identifying the position of the neutral region between Titan's magnetic lobes, Bertucci et al. (2007) concluded that the upstream flow was pointing away from Saturn at an angle of  $36^\circ$ . However, other authors suggested a number of different values for the direction of the upstream flow (Modolo et al., 2007a; Szego et al., 2007; Coates et al., 2012). Sittler et al. (2010) investigated CAPS data from T9 and suggested that the upstream plasma flow consisted mainly of light ( $H^+$ ,  $H_2^+$ ) ions. The upstream flow during T63 and T75 was approximately corotational (Coates et al., 2012).

By applying a hybrid model (kinetic ions and fluid electrons), Modolo et al. (2007a) were able to reproduce the locations of the split signatures measured by the Langmuir probe in the electron densities during T9. They needed an upstream plasma with a high mass density ( $O^+$  component with  $n(O^+) = 0.2 \text{ cm}^{-3}$ , as suggested by Neubauer et al., 1984) in order to do so. Hybrid modeling by Kallio

et al. (2007) showed that the magnetic field measurements during T9 can only be explained if the upstream plasma possesses such a high mass density. Hybrid modeling by Simon et al. (2007c) showed that the magnetic field topology measured during the T9 encounter is very robust against changes of the ionospheric SUV production rate and that a rotation of the ambient flow direction away from Saturn by  $34^\circ$  gives good agreement with the observed magnetic data. Ma et al. (2007) showed that applying a Hall-MHD model is suitable to reproduce magnetic perturbations seen during the flyby. These authors also showed that without a heavy upstream plasma component (16 amu) the magnetic data cannot be reproduced. However, their model did not succeed in generating the split signature and showed only a single peak in the electron density that was located in-between the two segments of the split tail.

Subsequently, Lipatov et al. (2012) applied a hybrid model with an upstream plasma consisting only of  $H^+$  ions and showed that using a high density ( $n(H^+) = 0.1 \text{ cm}^{-3}$ ) plasma or a low density ( $n(H^+) = 0.02 \text{ cm}^{-3}$ ) plasma with high beta produces similar results for the T9 flyby. They were able to quantitatively reproduce the ion densities measured in the first event; however, their modeling produced a higher density during the second event and no density gap in-between the two events. Their model also failed to simultaneously reproduce the magnitudes and locations of the magnetic draping signatures.

However, Lipatov et al. (2012) assumed that the incident magnetospheric ions moved at super-corotational speed ( $\sim 125\%$  the nominal corotation speed at Titan), which is inconsistent with the ambient magnetic field observations during T9. During this flyby the magnetometer detected a field line orientation that was swept back with respect to a strictly corotating meridional plane (i.e.,  $B_{0,x} > 0$ ,  $B_{0,y} > 0$  in TIS coordinates). According to Bertucci et al. (2009) and Simon et al. (2010) (see Figure 4 in that work), this implies that the incident plasma was in a state of subcorotation.

Several authors proposed that the split signatures seen in Titan's tail region during T9 may be related to non-stationarities or in the incident magnetospheric flow conditions on the length and time scales of the encounter (Modolo et al., 2007a; Bertucci et al., 2007). However, the subsequent detection of these features during T63 and T75 suggests that the split signatures may indeed be a more common feature in Titan's plasma interaction region. The non-detection of these split signatures during numerous tail crossings may imply that the individual filaments of the split tail are quite narrow in diameter. This suggests that it might be fairly easy for Cassini to simply 'miss' these signatures during an encounter. So far the split signatures detected during the T63 and T75 encounters have not been the subject of any modeling.

In this study, we therefore conduct a systematic study of the split signatures in the ion densities downstream of Titan, focusing especially on the dependency of the locations, densities and extensions of the individual tail filaments on Titan's orbital position and the incident magnetospheric flow conditions. We are more interested in understanding the physics behind these split signatures than in reproducing the details of the observations. For all three flybys during which Cassini detected a split signature in Titan's tail, the incident magnetospheric flow conditions are poorly constrained. Especially for T9, conflicting information on the incident plasma composition and flow direction can be found in the literature (cf. Kallio et al., 2007; Modolo et al., 2007a; Sittler et al., 2010; Coates et al., 2012). As opposed to exploring the vast parameter space of upstream conditions to achieve the best possible agreement with the data as other studies have done (Kallio et al., 2007; Simon et al., 2007c; Modolo et al., 2007a; Lipatov et al., 2012), we rather focus on a few simple scenarios that permit straightforward access to the physical mechanisms leading to the generation of the split tails.

The paper is structured as follows: in Section 2 we describe the hybrid code and the model of Titan's ionosphere as well as the different simulation setups considered in this study. The results of our model runs are presented in Section 3, along with a discussion of their implications for Cassini observations in Titan's tail region. Our major findings are briefly summarized in Section 4.

## 2. Simulation model

### 2.1. Hybrid code AIKEF

To conduct this survey, we use the hybrid simulation code AIKEF (Adaptive-Ion-Kinetic-Electron-Fluid, Müller et al., 2011), which treats ions as particles, while electrons act as a massless, charge-neutralizing fluid. The hybrid approach therefore enables plasma simulations to cover kinetic effects of individual particles, such as the asymmetries associated with large ion gyroradii and different flow patterns of light and heavy plasma constituents. Thus, the hybrid approach is particularly suitable to study the filamented tail structures seen during T9, T63 and T75.

The hybrid code AIKEF has been used in previous studies for a wide range of plasma interaction scenarios throughout the solar system. Titan's interaction has been the subject of many of these extensive studies before. For example, Titan's plasma interaction during a crossing of Saturn's magnetopause throughout the T32 encounter was studied in real-time by Simon et al. (2009a). Using a hierarchical grid that permits a higher resolution in Titan's ionosphere, the fossilization of the magnetic field in the moon's ionosphere during this encounter (as observed by Cassini, Bertucci et al., 2008) was studied by Müller et al. (2010). Titan's interaction with the supersonic solar wind, recently observed for the first time during T96 (Bertucci et al., 2015), was analyzed by Simon (2009). Simon and Motschmann (2009) studied the asymmetries of Titan's induced magnetosphere as a function of the moon's distance to Saturn's magnetodisk current sheet. AIKEF was also applied to study the plasma interactions of numerous other Saturnian moons visited by Cassini, e.g., Tethys (Simon et al., 2009b), Rhea (Roussos et al., 2008; Simon et al., 2012) and Dione (Krupp et al., 2013). Kriegel et al. (2011, 2014) included the effects of negatively charged dust grains on the plasma flow, which proved to be essential for the description of Enceladus's dusty plasma interaction.

A detailed discussion of the underlying equations and components of AIKEF is given by, e.g., Bagdonat (2005) and Kriegel (2014), however, a brief overview will be given here as well. Since it is not possible to store the phase space coordinates of  $\sim 10^{28}$  individual particles, the hybrid model treats the ions as macroparticles with the same mass-to-charge ratio as the real individual particles. The motion of these particles is therefore governed by the Lorentz force arising from the electromagnetic fields  $\underline{E}$  and  $\underline{B}$ , with equations of motion that read:

$$\frac{d\underline{x}_j}{dt} = \underline{v}_j, \quad \frac{d\underline{v}_j}{dt} = \frac{q_j}{m_j}(\underline{E} + \underline{v}_j \times \underline{B}), \quad (1)$$

where  $\underline{x}_j$ ,  $\underline{v}_j$ ,  $m_j$  and  $q_j$  denote the position, velocity, mass and charge of a single macroparticle.

With the assumption of negligible electron inertia (electron mass  $m_e \approx 0$ ) and plasma resistivity  $\eta \approx 0$ , the electron momentum equation reads

$$0 = -(\underline{E} + \underline{u}_e \times \underline{B}) - \frac{1}{en_e} \nabla P_e. \quad (2)$$

In this equation,  $\underline{u}_e$ ,  $n_e$  and  $P_e$  are the electron bulk velocity, electron number density and electron pressure, respectively. We introduce the charge-averaged ion quantities

$$\underline{u}_i = \frac{\sum_j q_j n_j \underline{u}_j}{en_e} \quad \text{and} \quad \rho_{c,i} \equiv en_e = \sum_j q_j n_j, \quad (3)$$

where the summation is carried out over all positive ion species, and  $\underline{u}_j$  and  $n_j$  denote the bulk velocity and number density of the respective ion species. Using the definition of the current density,  $\underline{j} = -en_e \underline{u}_e + \sum_j q_j n_j \underline{u}_j$ , as well as Ampère's law,  $\nabla \times \underline{B} = \mu_0 \underline{j}$  (where we neglect displacement currents  $0 \approx (1/c^2)(\partial \underline{E}/\partial t)$ ), one can derive an expression for the electric field from Eq. (2):

$$\underline{E} = -\underline{u}_i \times \underline{B} + \frac{(\nabla \times \underline{B}) \times \underline{B}}{\mu_0 \rho_{c,i}} - \frac{\nabla P_e}{\rho_{c,i}}, \quad (4)$$

where  $\rho_{c,i}$  is the total charge density of the ions. For the electron pressure we use an adiabatic equation of state given by

$$P_e = P_{e,0} \left( \frac{n_e}{n_{e,0}} \right)^\kappa, \quad (5)$$

with the adiabatic exponent  $\kappa=2$ , representing two degrees of freedom for electrons in a magnetized plasma (Böswetter et al., 2004). The quantities  $P_{e,0}$  and  $n_{e,0}$  are background parameters describing the undisturbed upstream plasma. An adiabatic description of the electrons had also been applied in the hybrid models of Modolo et al. (2007a) and Lipatov et al. (2012), who successfully described aspects of the split signatures detected during T9.

By applying Faraday's law to the electric field equation, one obtains an expression for the time evolution of the magnetic field

$$\frac{\partial \underline{B}}{\partial t} = \nabla \times \left[ \underline{u}_i \times \underline{B} \right] - \nabla \times \left[ \frac{(\nabla \times \underline{B}) \times \underline{B}}{\mu_0 \rho_{c,i}} \right], \quad (6)$$

where the electron pressure term vanishes in this equation due to the adiabatic description (Simon et al., 2007a). Negative ions (Coates et al., 2007a) are not included in this model.

## 2.2. Ionosphere model

The model for the ionosphere of Titan used in this paper has been drastically improved compared to the one used in our previous studies (e.g., Simon et al., 2006, 2007c; Müller et al., 2010) in several important respects. We describe Titan's ionosphere with a seven-species model, considering the same components as the MHD model by Ma et al. (2004, 2006) and the hybrid model by Ledvina et al. (2012). The model covers masses from 2 to 74 amu and accounts for the fact that the complex ion–neutral chemistry in Titan's ionosphere produces a vast number of different ion species, which are found to cluster around several distinct mass values (Cravens et al., 2006). An overview of the species included in the model is given in Table 1. The most abundant ion species observed in Titan's upper ionosphere ( $> 1000$  km),  $C_2H_5^+$  and  $HCNH^+$  (Krasnopolsky, 2009) are each represented by a separate model ion species. In each time step, ions of the first three model species ( $L^+$ ,  $M^+$ , and  $H1^+$ ) are added to the ionosphere in the simulation according to their total ion production rates, taking into account photoionization and impact ionization by magnetospheric electrons. We use the EUVAC model developed by Richards et al. (1994) to calculate realistic photoionization rates for these species. The EUVAC model provides wavelength-dependent solar UV radiation intensities at 1 AU,  $I_{\text{Earth}}(\lambda_i)$ , in the range of 50–1000 Å. This wavelength interval is divided into 37 wavelength bins and the intensity of the solar flux is scaled to account for the variability of the solar activity in the solar cycle. Our model includes three neutral species that are used for photoionization:  $H_2$ ,  $CH_4$  and  $N_2$ . The density profiles of these main components of Titan's neutral atmosphere are adopted from Cui et al. (2009) and are assumed to be spherically symmetric. Close to Titan,  $N_2$  and  $CH_4$  dominate the

**Table 1**

Ionospheric species used in the model with respective mass of the species in the code and the mass range of the corresponding physical species. Species which possess similar mass are grouped into a single species. Based on Ma et al. (2004).

Model species name	Physical composition	Mass	Mass range
$L^+$	$H^+, H_2^+$	2	1–2
$M^+$	$CH_5^+, CH_4^+, CH_3^+, CH_2^+, CH^+, C^+, N^+$	14	12–17
$H1^+$	$C_2H_5^+$	29	29
$H2^+$	$HCNH^+$	28	28
$MHC^+$	$C_3H^+, C_3H_2^+, C_3H_3^+, C_3H_4^+, C_3H_5^+, C_4H_3^+, C_4H_5^+$	44	37–53
$HHC^+$	$C_5H_3^+, C_5H_5^+, C_5H_7^+, C_5H_9^+, C_6H_5^+, C_6H_7^+, C_7H_5^+$	70	63–89
$HNI^+$	$C_3H_2N^+, C_5H_5N^+, C_3HN^+$	74	51–79

neutral atmosphere, however at high altitudes ( $\sim 2000$  km), hydrogen becomes the dominant species due to its large scale height ( $H_{H_2} \sim 300$  km compared to  $H_{N_2, CH_4} \sim 70$ – $90$  km). Photoionization of  $H_2$  is associated with the  $L^+$  species, of  $CH_4$  with the  $M^+$  species and of  $N_2$  with the  $H1^+$  species. All three neutral species are assumed to attenuate the solar flux in Titan's atmosphere by absorption of solar radiation. The total photoionization production rate  $P_{ph,j}(\underline{x}_0)$  for ion species  $j = \{L^+, M^+, H1^+\}$  at a position  $\underline{x}_0$  in Titan's upper atmosphere is therefore given by

$$P_{ph,j}(\underline{x}_0) = \sum_{i=1}^{37} \sigma_{ion,n}(\lambda_i) n_n(\underline{x}_0) I_{\text{Saturn}}(\lambda_i) \exp[-\tau(\underline{x}_0, \lambda_i)], \quad (7)$$

where we have introduced the optical depth

$$\tau(\underline{x}_0, \lambda_i) = \sum_n \sigma_{abs,n}(\lambda_i) \int_{\infty}^{\underline{x}_0} n_n(s) ds, \quad (8)$$

and  $\sigma_{ion,n}$ ,  $\sigma_{abs,n}$  and  $n_n$  denote the photoionization and absorption cross-sections and the density of the respective neutral species  $n = \{H_2, CH_4, N_2\}$ . The integration in Eq. (8) is carried out along the path element  $ds$ , which is along the straight line from the Sun to  $\underline{x}_0$ . The wavelength dependent photoabsorption and photoionization cross-sections are taken from Schunk and Nagy (2009). The solar flux at the topside of Titan's atmosphere  $I_{\text{Saturn}}(\lambda_i)$  is obtained by scaling of the EUVAC flux according to the distance of Saturn to the Sun,  $d(\text{Saturn})$  (in astronomical units), by

$$I_{\text{Saturn}}(\lambda_i) = I_{\text{Earth}}(\lambda_i) \frac{1}{d(\text{Saturn})^2}. \quad (9)$$

This method precisely describes the photoionization of Titan's atmosphere. It accounts for the local time and seasonal dependency of the location of the subsolar point and produces realistic ion production rates in the region around the terminator, in contrast to our preceding model (e.g., Simon et al., 2006). In the geometric shadow of Titan, the photoionization is zero. Thus, the ion production due to solar radiation is of a bowl-like shape and possesses rotational symmetry around the Sun–Titan line.

The model considers another source of ions for the ( $L^+$ ,  $M^+$ , and  $H1^+$ ) species associated with impact ionization by magnetospheric electrons. The respective ionization rates are taken from Ledvina et al. (2012) and added to the photoionization rate. According to the resulting production rates, ions are injected into the simulation during each time step. All other ionospheric species are generated solely as a result of ion–neutral reactions (see Table 2).

The ion–neutral interactions which are considered by our model include elastic collisions of the impinging magnetospheric plasma with Titan's three main neutral species ( $N_2$ ,  $CH_4$ , and  $H_2$ ), as well as the most important ion–neutral chemical reactions in the ionosphere. The elastic collision rates  $\nu_{in}$  are calculated by

$$\nu_{in} = \frac{2.7 \cdot 10^{-9} n_n (\alpha_n \mu_{in})^{0.5}}{m_i}, \quad (10)$$

where we apply  $\alpha_{H_2} = 0.82$ ,  $\alpha_{CH_4} = 2.59$  and  $\alpha_{N_2} = 1.76$  as the neutral polarizability parameters (Schunk and Nagy, 2009). The parameter  $\mu_{in}$  is the reduced mass of the reaction partners and  $m_i$  is the mass of the involved ion species.

The ion–neutral reactions which produce the other species in the ionosphere and their respective rate constants  $k_{in}$  are listed in Table 2. For any reactions that include a neutral species other than  $H_2$ ,  $CH_4$  or  $N_2$ , we assume a constant ratio  $\eta_n = n_n/n_{CH_4}$  of the respective species and  $CH_4$  in order to be able to calculate the process rate  $\nu_{in} = k_{in}n_n$  of the reaction. These minor species are only needed for the calculation of the chemical reactions and do not possess a fine structure (e.g., a local maximum) in their density profile above 900 km altitude. The mixing ratios of the minor neutral species are estimated from the density profiles given by Ledvina et al. (2012).

The numerical realization of the chemical reactions is done in a purely statistical way, with the method introduced by Krieger et al. (2011). A detailed description of the numerical mechanism for the chemical reactions is provided in that preceding paper. During each time step, reaction probabilities for every particle in the simulation are calculated. The reaction probabilities are related to the lifetime of a particle: the lifetime of an ion, i.e., the time between two reactions, is a random variable which is distributed exponentially. The probability that a particle does *not* undergo a reaction for the next time interval  $t$  is given by

$$P(t) = \exp\left(-\frac{t}{\tau_{in}}\right), \quad (11)$$

where  $\tau_{in}$  is the average time between two reactions. The probability that a particle will undergo a reaction during the next time interval  $\Delta t$  is therefore related to the reaction rate  $\nu_{in} = 1/\tau_{in}$  and given by  $p\Delta t$ , where

$$p = \frac{d}{dt}(1 - P(t))|_{t=0} = \nu_{in} = k_{in}n_n. \quad (12)$$

In the numerical model, the product  $p\Delta t$  is then compared against a random number  $r$  between 0 and 1 to decide if a reaction occurs (reaction:  $p\Delta t > r$ , no reaction:  $p\Delta t < r$ ). This approach requires the timestep  $\Delta t$  to be such that  $p\Delta t$  is much smaller than 1. If this condition is not fulfilled, the method is not implemented correctly.

During a reaction, an ion of the original species is removed from the simulation and replaced by an ion of the product species. New ions are initialized with the velocity of the neutral reaction partner, which we assume to have a temperature of 150 K in our simulations. No bulk velocity of the neutral species is assumed in our model. Since these neutral velocities ( $\sim 1$  km/s) are negligible compared to the plasma velocities ( $\sim 100$  km/s), the chemical reactions as well as collisions effectively slow the overall plasma down. If an elastic collision occurs, the ion remains in the simulation and its velocity is changed to that of the neutral collision partner.

### 2.3. Simulation setup and numerical parameters

In our simulations we use a box with an extension of  $20 R_T \times 20 R_T \times 20 R_T$ , where the center of the box coincides with the center of Titan. A hierarchical grid with one level of refinement is used, the spatial resolutions of which are  $L_0 = 0.25 R_T$  and  $L_1 = 0.125 R_T$ . The region of high refinement is located within a cube of  $2 R_T \times 2 R_T \times 2 R_T$  around the center of Titan, containing the ionosphere. In all simulation runs, we use two magnetospheric upstream species,  $O^+$  and  $H^+$ , with  $n(O^+) = 0.2 \text{ cm}^{-3}$ ,  $n(H^+) = 0.1 \text{ cm}^{-3}$ . The upstream flow direction is always corotational. The upstream species are initialized with 40 particles in every cell at the beginning and at the outer boundaries during the simulations. The inner boundary is set to 1000 km above the surface during all runs. If a particle reaches the inner boundary, it is removed from the simulation.

The plasma parameters for the simulation runs presented in this paper are summarized in Table 3. To permit straightforward access to the physics of the split signatures in Titan's tail, we first consider an idealized geometry, where the upstream flow direction is aligned with the  $x$ -axis and the ambient magnetic field is aligned with the  $-z$  axis (Run #1 in Table 3). In the literature, this setup is often referred to as the 'Voyager 1 scenario' of the Titan interaction (Simon et al., 2009a).

For the T9 case (Run #2 in Table 3) there has been a lot of discussion about the direction and composition of the upstream

**Table 2**

Ion–neutral reactions included in the model. Rate constants  $k_{in}$  are taken from Krasnopolsky (2009) and Vuitton et al. (2007).

Reaction	$k_{in}$ ( $10^{-10} \text{ cm}^3/\text{s}$ )
$CH_3^+ + C_2H_4 \rightarrow C_2H_5^+$	15.0
$C_2H_5^+ + HC_3N \rightarrow HC_3NH^+$	36.0
$CH_3^+ + C_2H_6 \rightarrow C_2H_5^+$	2.0
$HCNH^+ + C_4H_2 \rightarrow C_4H_3^+$	1.8
$N^+ + CH_4 \rightarrow HCNH^+$	4.0
$HCNH^+ + HC_3N \rightarrow HC_3NH^+$	34.0
$CH_3^+ + CH_4 \rightarrow C_2H_5^+$	11.0
$C_3H_5^+ + C_2H_2 \rightarrow C_5H_5^+$	3.8
$C_2H_5^+ + HCN \rightarrow HCNH^+$	27.0
$C_3H_5^+ + C_2H_4 \rightarrow C_5H_5^+$	5.5
$C_2H_5^+ + C_2H_2 \rightarrow C_3H_3^+, C_4H_3^+$	1.9
$C_4H_3^+ + C_4H_2 \rightarrow C_6H_3^+$	7.4
$C_2H_5^+ + C_2H_4 \rightarrow C_3H_5^+$	3.5

**Table 3**

Plasma parameters of the simulation runs.

Quantity	Symbol	Run #1	Run #2	Run #3
Local time	LT	18:00	3:00	17:00
Latitude of subsolar point	SSL (deg)	0	−19.06	−2.04
Upstream magnetic field vector	$\underline{B}_0$	(0,0,−5)	(3.73,4.7,−2.15)	(0.05,−0.33,−4.48)
Upstream magnetic field strength	$B_0$ (nT)	5	6.37	4.49
Number density of upstream $O^+$	$n_{0,O^+}$ ( $\text{cm}^{-3}$ )	0.2	0.2	0.2
Number density of upstream $H^+$	$n_{0,H^+}$ ( $\text{cm}^{-3}$ )	0.1	0.1	0.1
Upstream plasma bulk velocity	$U_0$ (km/s)	120	120	120
Alfvénic Mach number	$M_A$	1.96	1.54	2.22
$O^+$ gyration period	$\Omega_0^{-1}$ (s)	33	26	37

plasma flow. While the consensus was that the flow deviated from the corotational direction, a number of different values for the angle of this deviation have been proposed in numerical and observational studies (Bertucci et al., 2007; Modolo et al., 2007b; Szego et al., 2007). Also, Kallio et al. (2007), Simon et al. (2007c) and Ma et al. (2007) showed that in order to explain the magnetic signatures which were observed during T9, an upstream plasma with a high mass density ( $\sim 10^{-1}$  amu/cm<sup>3</sup>) is needed, in contrast to observational studies that showed no evidence of heavy ions (O<sup>+</sup>) in CAPS data (Sittler et al., 2010; Coates et al., 2012). Considering the typical electron number densities observed at Titan's orbital position (on the order of  $10^{-2}$  cm<sup>-3</sup>, cf. Arridge et al., 2011), such high mass density cannot be achieved by a plasma only consisting of H<sup>+</sup> and H<sub>2</sub><sup>+</sup>.

In summary, CAPS and MAG observations do not provide a consistent picture of the magnetospheric flow parameters during T9, and even different studies of CAPS data suggest conflicting values for the vector  $\underline{u}_0$ . Again, we are more interested in investigating the physics of the split signatures rather than in reproducing flyby data,

and therefore restrict ourselves to a corotational upstream flow direction with the same upstream composition as in the Voyager scenario, i.e.,  $n_{0,O^+} = 0.2$  cm<sup>-3</sup> and  $n_{0,H^+} = 0.1$  cm<sup>-3</sup> for all simulations (see Table 3). This upstream composition was also used by Kallio et al. (2007) and Simon et al. (2007c) to explain magnetometer data from T9. We also note that a statistical study of CAPS data from numerous crossings of Titan's orbit found the *average* radial and north–south components of the upstream flow direction to be negligible, compared to the azimuthal component (Arridge et al., 2011) at the location of Titan (see Table 6 in that work).

During T63 and T75, Titan's environment was distorted by the moon's proximity to Saturn's magnetodisk current sheet (Simon et al., 2013; Smith and Rymer, 2014). The magnetic signature of Titan's interaction during T63 and T75 was therefore partially obscured by magnetospheric fluctuations, whereas T9 was clearly located in the southern lobe of Saturn's magnetodisk. The chosen background magnetic field vector for T63 is therefore strongly dependent on the averaging intervals and not well constrained,

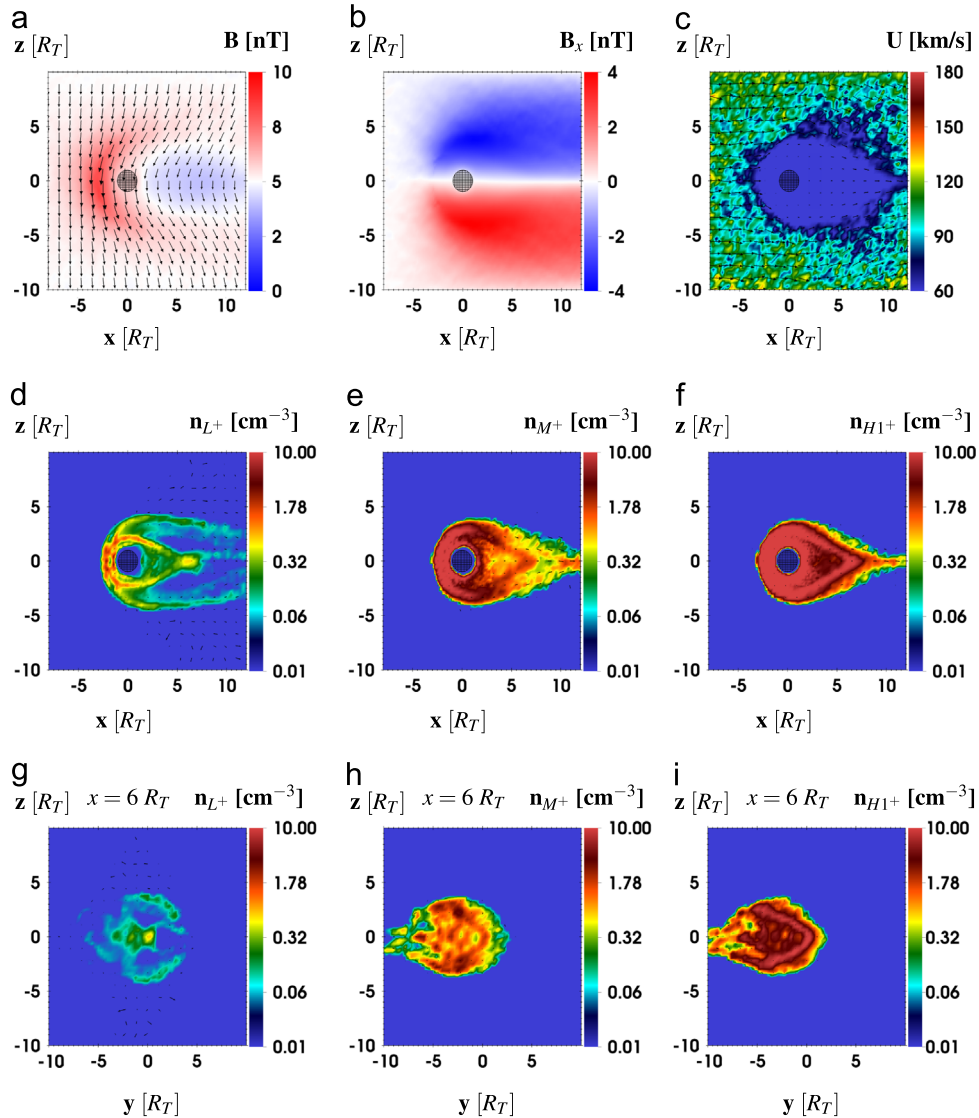


**Fig. 2.** Plasma quantities in the  $y=0$  plane for Run #1: (a) magnetic field strength, (b)  $B_x$  component, (c) total velocity magnitude  $|\underline{u}|$  (Eq. (3)), (d) ionospheric L<sup>+</sup> density, (e) ionospheric M<sup>+</sup> density, and (f) ionospheric H1<sup>+</sup> density. Quantities in  $x=6 R_T$  plane: (g) ionospheric L<sup>+</sup> density, (h) ionospheric M<sup>+</sup> density, and (i) ionospheric H1<sup>+</sup> density. Arrows indicate velocities of respective ion species ( $\underline{u}_i$ ) or the quantity itself ( $\underline{B}$ ,  $\underline{u}_i$ ).

whereas for T9 the background magnetic field has a far more quiet structure.

### 3. Results

#### 3.1. Run #1: Voyager-type upstream conditions

First we look at the ‘canonical’ Voyager scenario (Run #1 in Table 3). In this run, the dayside ionosphere coincides with the ramside of the moon and the convective electric field points in the  $-y$  direction. Important upstream plasma quantities and the densities of the  $L^+$ ,  $M^+$  and  $H1^+$  species are plotted in Fig. 2.

Fig. 2 (a) shows the magnetic field strength with a pileup upstream of Titan of  $\sim 8$  nT (undisturbed value  $B_0 = 5$  nT) and a decreased field in the magnetic wake downstream of Titan with a value  $\sim 3.5$  nT. The draping of the magnetic field is seen in the  $B_x$  component in Fig. 2(b), where the  $B_x$  component is negative in the northern lobe and positive in the southern lobe, reaching values of  $\pm 3.25$  nT (from  $B_{0,x} = 0$ ). The draping is symmetric with respect to  $z=0$  in this plane. As can be seen from Fig. 2(c), the plasma velocity  $|\underline{u}_i|$  is greatly reduced from its upstream value of  $\underline{u}_0 = 120$  km/s to a few m/s in the vicinity of Titan, starting at  $x \approx -4$ . The region of reduced flow speed possesses an extension of up to  $8 R_T$  along the  $z$ -axis, due to collisions and mass-loading of cold ionospheric ions.

Compared to our previous simulations (e.g., Simon et al., 2006), the effective size of the obstacle is increased by about  $\sim 2$ – $3 R_T$  due to the large region around Titan where slow ionospheric ions reduce the mean plasma velocity, leading to a broader and more diffuse pileup and draping pattern of the magnetic field. Fig. 2(d)–(f) shows the structure of the ionospheric tail in the plane parallel to the background field  $B_0$ , revealing a different behavior between the light species ( $L^+$ ) and the heavy species ( $M^+$  and  $H1^+$ ). The light ion species in Fig. 2(d) shows a symmetric split tail in the  $y=0$  plane with four escape paths near Titan ( $x < 6 R_T$ ) and only three further away downstream ( $x > 6 R_T$ ). The split tail consists of two outer filaments visible at  $z = \pm 5 R_T$  and two inner filaments at  $z = \pm 2 R_T$ , which merge into a single tail along  $z=0$  with densities comparable to or larger than the upstream plasma density. The two outer filaments have a thickness of less than  $1 R_T$  in  $z$  direction and become more diffuse with increasing distance to Titan. The heavy species in Fig. 2(e) and (f) shows two broader filaments (thickness  $1$ – $2 R_T$ ) which merge at a similar distance in the  $z=0$  plane. These structures correspond to the *inner* filaments seen in the  $L^+$  species, but no outer filaments are formed.

The formation of the outer filaments in the light species can be understood as follows: Due to the electron pressure gradient force pointing away from Titan, newly generated ions are accelerated radially away from the moon. A fraction of these ions then move along the draped magnetic field lines and escape into the region of Titan’s magnetic lobes as they are transported downstream, which produces the two outer filaments at  $z = \pm 5 R_T$  in the density pattern of the light ion species ( $L^+$ ). The heavier ionospheric species (Fig. 2(e) and (f)) are in principle susceptible to the same escape mechanism. However, since the light neutral species has a larger scale height than the heavy species ( $H_{H_2} \sim 300$  km compared to  $H_{N_2,CH_4} \sim 70$ – $90$  km), the region where light  $L^+$  ions are produced penetrates deeper into the region of draped field lines than the region where  $M^+$  and  $H1^+$  ions are produced. Therefore the fraction of light ions escaping along the draped field lines is much larger than the fraction of intermediate ( $M^+$ ) and heavy ions ( $H1^+$ ). For this reason the two outer filaments are absent in the density patterns of the heavier species (Fig. 2(e) and (f)).

The ions generated at lower altitudes form the two inner filaments, which are seen in all ionospheric species. Since the ion

production rates of the heavy species are at least one order of magnitude higher than that of the light ions, the inner filaments of the heavy species (Fig. 2(e) and (f)) have a higher density (factor  $\sim 10$ ) and are broader ( $1$ – $2 R_T$  compared to less than  $1 R_T$ ). The inner filaments are mainly associated with the transport of ions from the ramside towards downstream, i.e., these filaments first ‘drape’ around Titan and are then focused into the magnetic wake, merging to a single tail at a certain distance (at  $x \sim 6$ – $7 R_T$  in this simulation) along the  $x$ -axis in the  $z=0$  plane. This yields a triangular escape pattern in the  $y=0$  plane with a region of decreased density inside (factor of  $\sim 10$  compared to the filaments). In Run #1 the dayside ionosphere coincides with the ramside ( $18$  Saturnian local time), so that most of the ions are produced at the ramside and have to pass Titan to reach the wake.

For the  $x=6 R_T$  plane, Fig. 2(g)–(i) depicts the densities of the ionospheric species to illustrate the extent and structure of the outer filaments perpendicular to the magnetic field. In this plane, the outer filaments of the light  $L^+$  species in Fig. 2(g) have a parabolic shape that cover the region of a half-circle ( $-2 R_T < y < 4 R_T$  and  $-4 R_T < z < 4 R_T$ ), and are discontinuous perpendicular to the magnetic field (along  $z=0 R_T$ , cf. Fig. 2(g)). They have a thickness of less than  $1 R_T$ , which is the same extension as already seen in the  $y=0$  plane of Fig. 2(d). The outer filaments are mostly seen on the Saturn-facing side ( $y > 0 R_T$ ). On the Saturn-averted side ( $y < -2 R_T$ ) no parabolic filament structure can be identified, since the pick-up motion of the ions is going into that direction, as can be seen by the asymmetry in the ion density distribution towards  $y < 0$  in Fig. 2(g)–(i). Since the outer filaments of the light  $L^+$  species have a small thickness and are mainly located in planes that are defined by the unperturbed convective electric field  $\underline{E}_0 = \underline{u}_0 \times \underline{B}_0$ , it would be easy for a spacecraft to miss them. For the Voyager-type upstream conditions just discussed, a spacecraft would have needed to move mainly in the  $z$  direction to be able to detect the outer filaments of the light species. Spacecraft trajectories that are not roughly aligned with the magnetic background field  $B_0$  cannot observe both of the split tail filaments, only one part of them.

The quantities for the equatorial  $z=0$  plane are shown in Fig. 3. The magnetic field pile up shown in Fig. 3(a) is shifted towards  $y < 0$  (see also Simon et al., 2006). No draping pattern can be seen in the  $B_x$  component in Fig. 3(b), since the  $z=0$  plane coincides with the neutral plane of the draped field. The area of decreased plasma velocity in Fig. 3(c) is also shifted towards  $y < 0$ , due to the cycloidal motion of pickup ions into that direction. The pickup tail of the  $L^+$ ,  $M^+$  and  $H1^+$  species is seen in Fig. 3(e)–(f). Newly generated ions escape on cycloidal trajectories in the direction of the convective electric field, forming an asymmetric structure in the equatorial plane due to the large gyroradii which are on the order of several Titan radii. In this plane the tail also exhibits filament-like structures: Similar to the  $y=0$  plane, the transport of ions from Titan’s ramside to the wakeside generates a similar triangular region of decreased density downstream of the moon as seen in Fig. 2(d)–(f). However, this structure is asymmetric with respect to the direction of the convective electric field, i.e., it is frayed out.

Thus, the ionospheric tail of Titan possesses a quite complex structure. The densities in Titan’s pick-up tail are not homogeneous, but the ion escape mainly takes place in several narrow, filament-like channels. In the  $y=0$  plane (i.e., the plane defined by  $\underline{E}_0$ ), the tail is symmetric with respect to  $z=0$  and consists of four segments near Titan. Along the outer edges, only light ( $2$  amu) ions escape into the magnetic lobes. These outer filaments exhibit a parabolic shape in directions perpendicular to  $\underline{u}_0$ . However, the largest fraction of all species escape in two inner filaments from the dayside to the nightside and is focused into the magnetic wake at  $z=0$ .

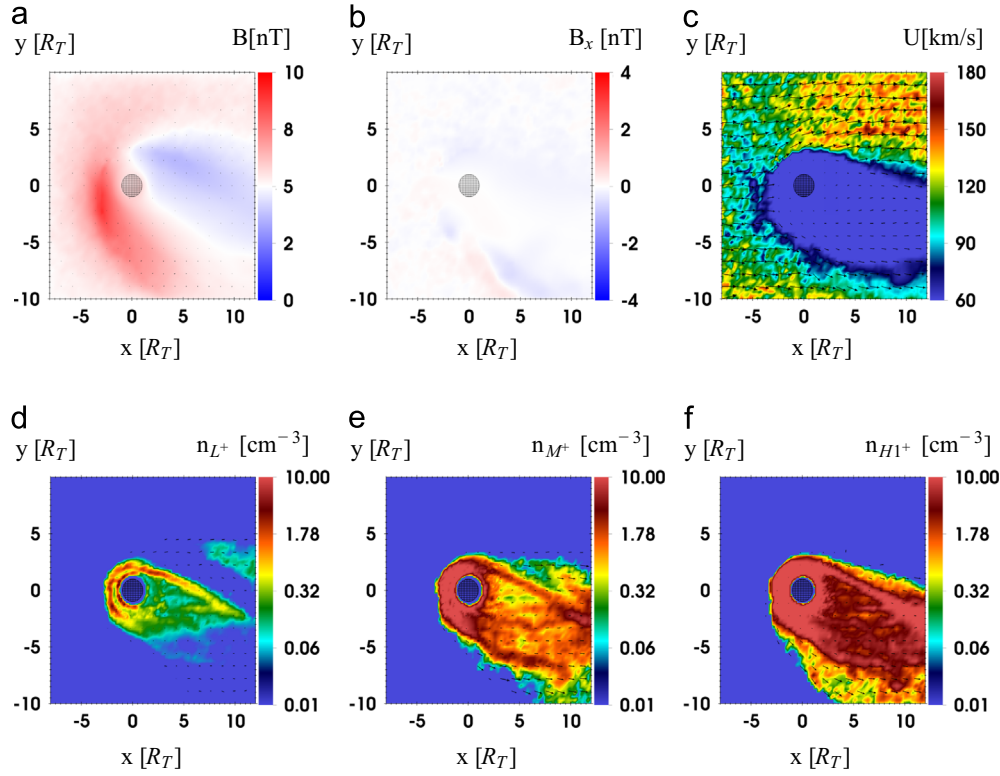


**Fig. 3.** Plasma quantities in the equatorial  $z=0$  plane for Run #1: (a) magnetic field strength, (b)  $B_x$  component, (c) total velocity magnitude  $|\underline{u}|$ , (d) ionospheric  $L^+$  density, (e) ionospheric  $M^+$  density, and (f) ionospheric  $H1^+$  density. Arrows indicate velocities of respective ion species ( $\underline{u}_i$ ) or the quantity itself ( $\underline{B}$ ,  $\underline{u}_i$ ).

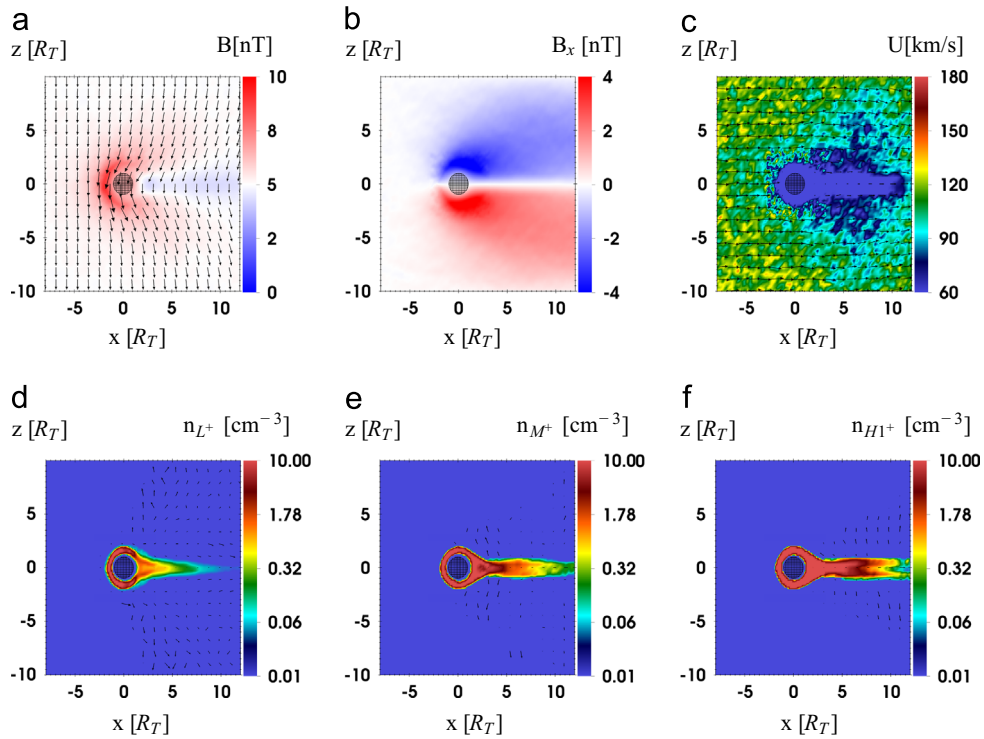


**Fig. 4.** Plasma quantities in the  $y=0$  plane for Run #1 with collisions and  $v_{Pe}$  term removed: (a) magnetic field strength, (b)  $B_x$  component, (c) total velocity magnitude, (d) ionospheric  $L^+$  density, (e) ionospheric  $M^+$  density, and (f) ionospheric  $H1^+$  density. Arrows indicate velocities of respective ion species ( $\underline{u}_i$ ) or the quantity itself ( $\underline{B}$ ,  $\underline{u}_i$ ).

Filamentation of the ionospheric tail is also seen in the  $z=0$  plane (defined by  $\underline{n} = \underline{B}_0$ ), however here the tail structures are asymmetric (shifted towards  $y < 0$ ) due to the large gyroradii of the pick-up ions. Combined, the inner filaments which are

associated with the transport of ions from the ramside to the wakeside form a cone structure behind Titan, pointing towards downstream. The surface of the cone consists of the inner filaments and inside the cone the density of the ionospheric species is

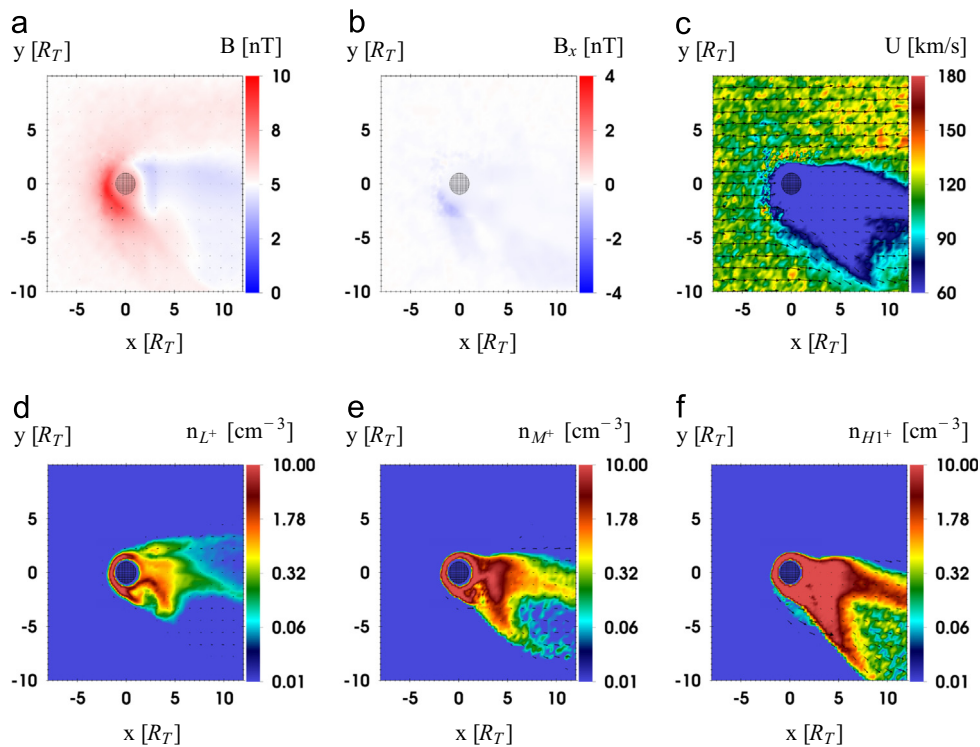


**Fig. 5.** Plasma quantities in the  $z=0$  plane for Run #1 with collisions and  $\nabla P_e$  term removed: (a) magnetic field strength, (b)  $B_x$  component, (c) total velocity magnitude, (d) ionospheric  $L^+$  density, (e) ionospheric  $M^+$  density, and (f) ionospheric  $H1^+$  density. Arrows indicate velocities of respective ion species ( $\underline{u}_i$ ) or the quantity itself ( $B$ ,  $\underline{u}_i$ ).

decreased compared to the surface. The apex of the cone is the point downstream of Titan, where the inner filaments merge to a single tail. Towards the direction of the convective electric field, the cone is ‘open’, or frayed out.

It is therefore possible to find trajectories that penetrate through different parts of the filament structures, leading to the detection of split signatures in the ion densities.

### 3.1.1. Run #1: collisions and $\nabla P_e$ removed

Now we consider the same upstream conditions as in Run #1, but this time with collisions and  $\nabla P_e$  term removed from the simulation. Apart from the more sophisticated ionosphere model, this setup is similar to what was done in our preceding studies (Simon et al., 2006, 2007b). We plot the same selection of quantities as in the previous section, for the  $y=0$  plane in Fig. 4 and the equatorial  $z=0$  plane in Fig. 5.

With no collisions and no  $\nabla P_e$  term in the electric field equation, the overall plasma interaction is confined to a narrower region than before, since the ionosphere is no longer inflated by the pressure gradient term and thus, the effective size of the obstacle is much smaller. This is indicated by the region of reduced plasma velocity around Titan in Fig. 4(c), which is by a factor of  $\sim 2$  smaller than in the previous run (Fig. 2(c)). With no collisions and the  $\nabla P_e$  term removed, the magnetospheric ions are not slowed down in Titan’s neutral atmosphere, and the cold ionospheric ions are not accelerated radially away from Titan, so that the region of decreased plasma velocity around Titan is not inflated.

Bagdonat (2005) found a similar impact of the pressure gradient term in hybrid simulations of the solar wind interaction of comet 67P/Churyumov-Gerasimenko. This author showed that the pressure gradient term tends to extend the region of high heavy ion density around the comet, thereby also increasing the size of the region where the Solar Wind is deflected and decelerated.

Consequently, the pileup of the magnetic field in Fig. 4(a) is slightly increased with  $\approx 9$  nT compared to before ( $\approx 8$  nT) due to the more pronounced draping of the magnetic field around Titan.

The outer filaments of the light species vanish (Fig. 4(d)) since no ions are accelerated radially away from the moon, i.e., the region at Titan’s ramside where the region of slow ionospheric particles intersects the draped magnetic field is much smaller than in the preceding case. The cone structure formed by the inner filaments is not visible anymore (Fig. 4(d)–(f)), as the ions generated on the ramside pass Titan at a much closer distance and the two streams merge immediately downstream of Titan into a single narrow tail. The tail formed by the heaviest species shows some tendency to split up at large distances to Titan: the only split tail structure that can be identified here is confined to the equatorial plane, where one filament is filling the magnetic wake (at  $y=0$  in Fig. 4(d)–(f), and another filament (Fig. 4(e) and (f)) is seen on the  $y < 0$  side, associated with the cycloidal motion of the pick-up ions. However, there is no Cassini flyby that could confirm the existence of this feature.

### 3.2. Run #2: T9-type upstream conditions

During T9 the background magnetic field possessed large positive  $B_{0,x}$  and  $B_{0,y}$  components (Table 3) due to Titan’s location below Saturn’s magnetodisk (Bertucci et al., 2007). The field lines were swept back due to the corotation lag (Simon et al., 2010) and were bent towards Saturn. Since the corotational upstream flow is no longer perpendicular to the magnetic background field, the neutral sheet between Titan’s magnetic lobes becomes curved, i.e., the magnitudes and extensions in the moon’s northern and southern magnetic lobes are no longer symmetric. In addition, the asymmetry that arises from the large gyroradii (Simon and Motschmann, 2009) is still present. An overview of the upstream geometry and the orientation of important planes in TIIS coordinates is provided in Fig. 6. Since the upstream magnetic field is not aligned with the  $z$ -axis anymore, the tail as a whole is rotated, i.e., the quasi-cycloidal structures of the pick-up ions are not confined to the equatorial  $z=0$  plane as in the Voyager case (Run # 1), but instead to the inclined plane which is defined by the normal vector  $\underline{B}_0$  (cf. Fig. 6(b)).

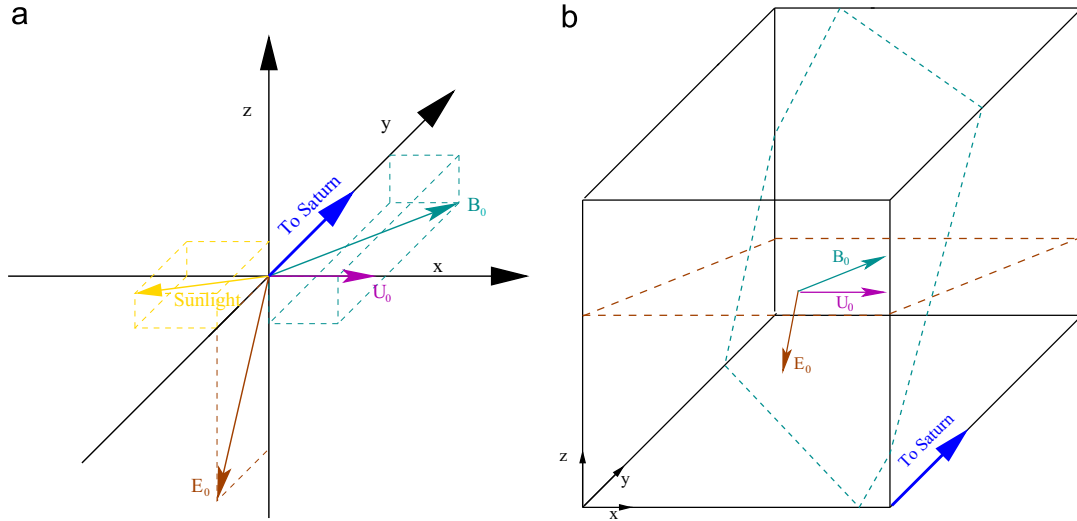


**Fig. 6.** (a) Upstream geometry of  $u_0$ ,  $B_0$  and  $E_0$  during the T9 encounter in the TIS coordinate system. (b) Orientation of the inclined planes defined by  $B_0$  (cyan plane) and  $E_0 = -u_0 \times B_0$  (brown plane) in the simulation box. (For interpretation of the references to color in this figure caption, the reader is referred to the web version of this paper.)

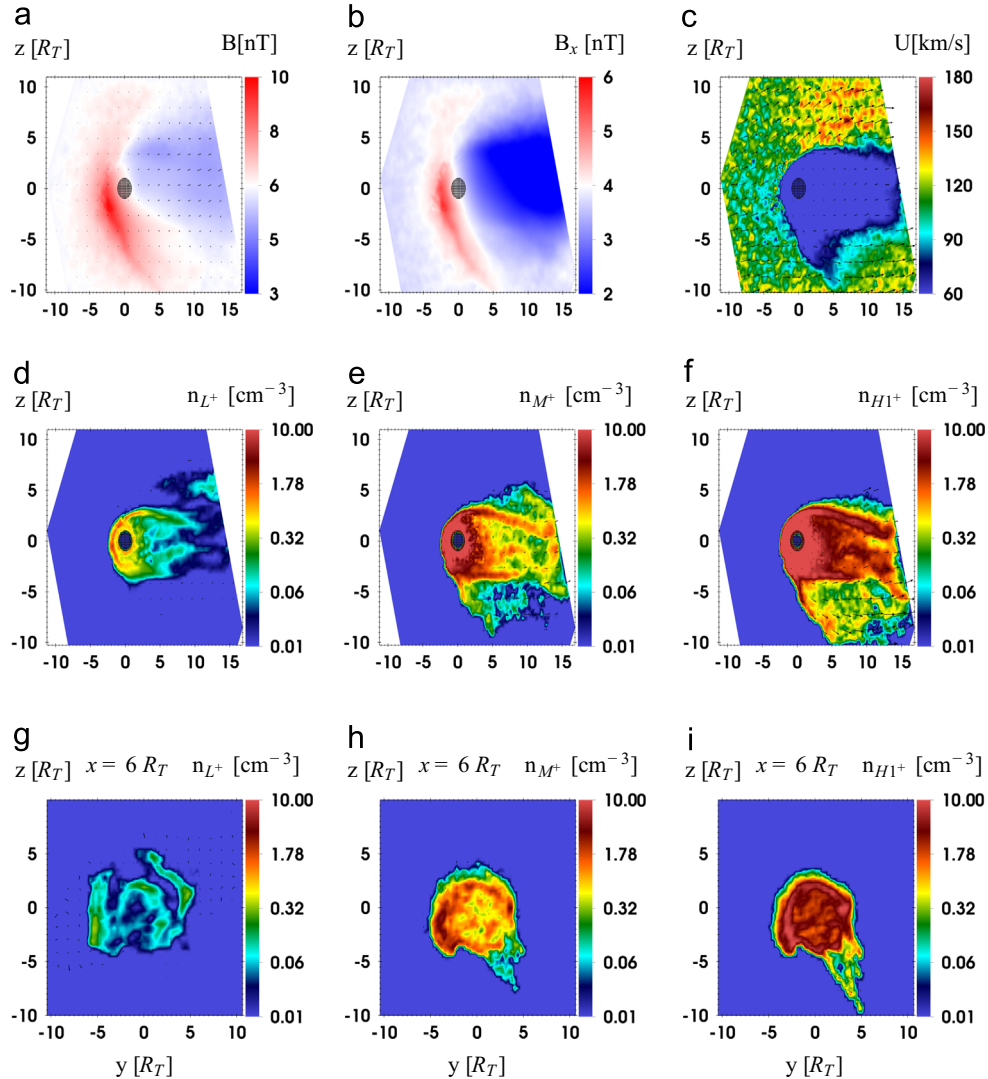


**Fig. 7.** Plasma quantities for Run #2 (T9) in the plane perpendicular to  $B_0$  (cyan plane in Fig. 6(b), axes are scaled in units of  $R_T$ ): (a) magnetic field strength, (b)  $B_x$  component, (c) total velocity magnitude, (d) ionospheric  $L^+$  density, (e) ionospheric  $M^+$  density, and (f) ionospheric  $H1^+$  density. Cut through the  $x=6 R_T$  plane: (g) ionospheric  $L^+$  density, (h) ionospheric  $M^+$  density, and (i) ionospheric  $H1^+$  density. Arrows indicate velocities of respective ion species ( $u_j$ ) or the quantity itself ( $B$ ,  $u_i$ ).

In Fig. 7(a)–(f) we show the plasma quantities in the plane perpendicular to the magnetic field, i.e., the plane defined by the normal vector  $\underline{n} = \underline{B}_0$  (cyan plane in Fig. 6(b)). This inclined plane includes an angle of about  $42^\circ$  with the  $y=0$  plane, which is why the sections in Fig. 7(a)–(f) have a non-quadratic shape. Also note that the drift velocity  $\underline{E}_0 \times \underline{B}_0$  is not parallel with  $\underline{u}_0$  (corotation) in this run, instead it also possesses components that are aligned with  $-z$  and  $-y$ . Fig. 7(a) shows the asymmetric pileup and wake structure, which is similar to Fig. 3(a). The  $B_x$  component of the magnetic field in Fig. 7(b), however, does not indicate the neutral plane of the draped magnetic field anymore as in Fig. 3(b), because of the rotated magnetic background. As expected, the asymmetric tail structures of the ionospheric species are seen in the plane perpendicular to the magnetic field (cf. Fig. 7(d)–(f)). Filaments (1–2  $R_T$  thickness) are visible at  $z \approx \pm 3 R_T$ , as well as smaller filaments (thickness less than one  $R_T$ ) for the  $M^+$  and  $H1^+$  species on the edge of the pick-up structures (towards  $z < 0$ ). However, no real cone structure is seen, as the filaments do not merge into a single tail similar to the plots in Fig. 3(d)–(f).

A cut through Titan's ionospheric tail at  $x=6 R_T$  is plotted in Fig. 7(g)–(i). Compared to the plots from Fig. 3(g)–(i) the filament structure is similar, but they are rotated clockwise by  $\sim 70^\circ$ , which

is roughly the angle between the T9 magnetic field and north-south magnetic field used in the Voyager scenario. The light  $L^+$  species shows the outer filament structures at  $y = \pm 5 R_T$  in Fig. 7(g), which are again asymmetric with respect to the direction of the pickup cycloids.

Fig. 8(a)–(f) shows the plasma quantities in the equatorial  $z=0$  plane, which is identical to the plane of the T9 trajectory (cf. Fig. 1). The draping pattern in Fig. 8(a) and (b) is asymmetric since the upstream magnetic field and flow direction are not perpendicular to each other (Simon and Motschmann, 2009). Fig. 8(g)–(i) depicts the densities of the ionospheric species in the plane defined by the convective electric field  $\underline{E}_0 = \underline{u}_0 \times \underline{B}_0$  (cf. brown plane in Fig. 6(b)), i.e., in the plane where the split structures are most pronounced corresponding to the  $y=0$  plane in the Voyager Run #1. For the selected set of upstream parameters, this plane is roughly coincident with the  $z=0$  plane, but is slightly rotated counter-clockwise around the  $x$ -axis by an angle of  $\sim 25^\circ$ . As we can see in Fig. 8(d)–(i), the tail is tilted with respect to the upstream flow direction  $\underline{u}_0$ .

The split tail of the light  $L^+$  species can be seen in both of these planes (cf. Fig. 8(d) and (g)). However, we do not see a clear four-filament structure as in Run #1; only three filaments can be identified in these plots. The region of decreased density between

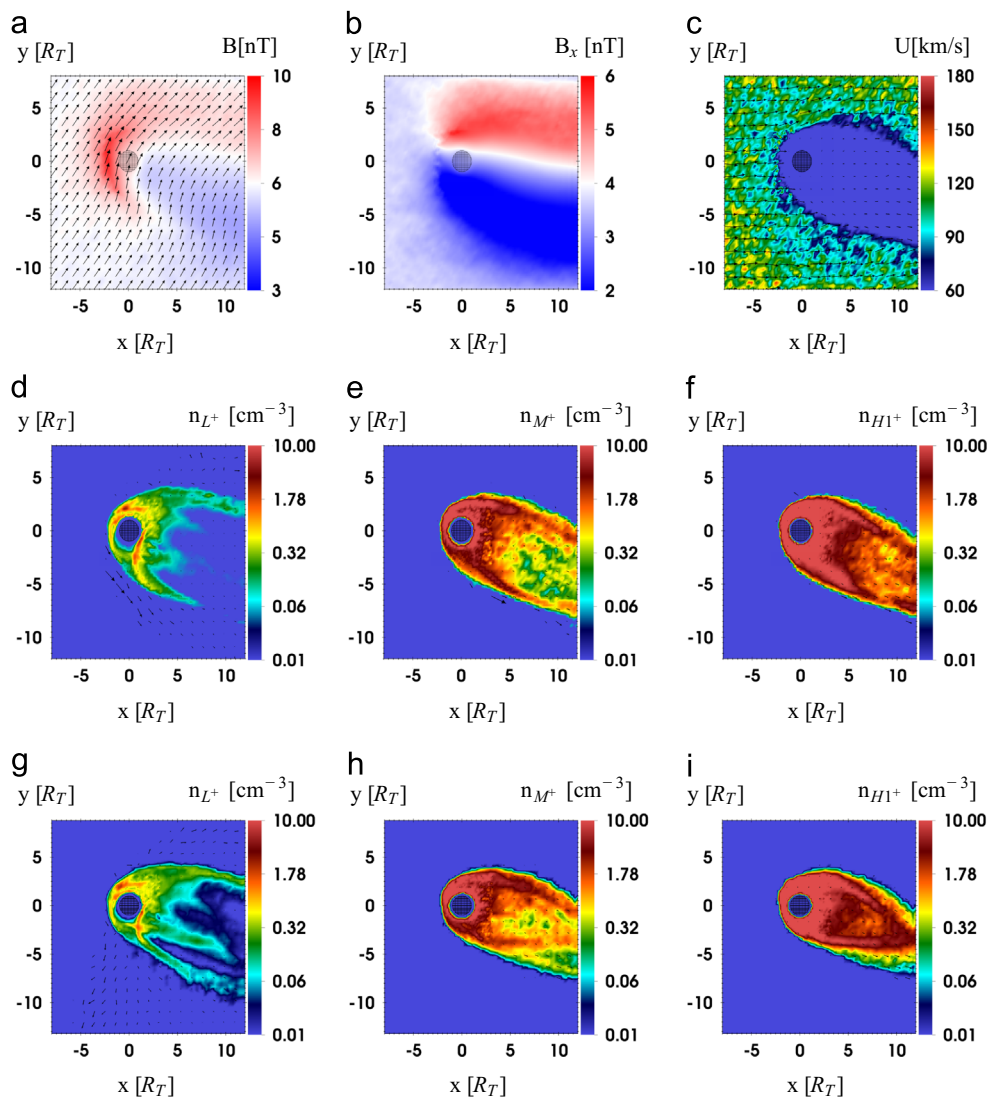


**Fig. 8.** Plasma quantities for Run #2 (T9) in the equatorial  $z=0$  plane: (a) magnetic field strength, (b)  $B_x$  component, (c) total velocity magnitude, (d) ionospheric  $L^+$  density, (e) ionospheric  $M^+$  density, and (f) ionospheric  $H1^+$  density. Inclined plane defined by  $\underline{E}_0 = \underline{u}_0 \times \underline{B}_0$  (brown plane in Fig. 6(b)): (g) ionospheric  $L^+$  density, (h) ionospheric  $M^+$  density, and (i) ionospheric  $H1^+$  density. Arrows indicate velocities of respective ion species ( $\underline{u}_j$ ) or the quantity itself ( $\underline{B}$ ,  $\underline{u}_i$ ).

the two outer filaments of the light  $L^+$  species in Fig. 8(d) and (g) has a diameter of up to  $7 R_T$ , which is equivalent to 50 min of travel time for typical Cassini velocities near Titan (6 km/s). As we would expect, the split tail is most pronounced in the plane that includes both  $\underline{B}_0$  and  $\underline{u}_0$  (cf. Fig. 8(g)), where it reaches the downstream boundary of the simulation box. In the equatorial  $z=0$  plane (Fig. 8(d)), however, only the Saturn-facing filament reaches the wakeside boundary of the simulation box, whereas the Saturn-averted filament bends out of this plane much closer to Titan. This information can be used to obtain an estimation of the length of these parabolic filaments in the plane that contains  $\underline{E}_0$  and  $\underline{B}_0$ . If we consider a point (e.g.,  $(5, -7.0)R_T$ ) where the Saturn-averted filament breaks off in Fig. 8(d) and the angle between the two planes ( $25^\circ$ ), by using simple geometry we derive an upper limit of  $\sim 3 R_T$  on the half width of these filaments in this plane, which is a good approximation if we compare it against the cut through the tail in Fig. 8(g).

On the Saturn-facing side ( $y > 0$ ) the filaments are slightly thicker and more dense, compared to the Saturn-averted ( $y < 0$ ) side. Since the upstream flow is corotational (from  $-x$  to  $+x$ ) and the draped magnetic field lines are more aligned with the upstream flow in the  $y > 0$  halfspace (see Fig. 8(a)), it is ‘easier’ for the ions to move into the Saturn-facing segment of the tail. The local time of the encounter further enhances this effect, since Titan’s dayside ionosphere during T9 is located in the middle of the  $+x+y$ -quadrant (the orbital position of Titan was at 3 LT, so the terminator line is at a  $45^\circ$  angle with the  $x$ - and  $y$ -axis in TIIS coordinates, cf. Fig. 6(a)). This means more ions are produced on the Saturn-facing side (dayside) than on the Saturn-averted side (nightside) of Titan. Based on the picture from Fig. 2(d), it seems that the upper outer and inner filaments of the light species merged (from the symmetric case) into one larger filament due to the asymmetric upstream geometry in combination with the location of the dayside ionosphere during T9.

Let us now look at the ion densities of the  $L^+$  and  $M^+$  species along several hypothetical trajectories as well as along the T9 trajectory, plotted in Fig. 9, to understand the densities in the tail from a spacecraft point of view. Density profiles of the heavy species  $H1^+$  are not shown, as they are very similar to the densities of the  $M^+$  species. The hypothetical trajectories are all parallel to the  $y$ -axis and have different fixed  $x$  and  $z$  coordinates, therefore representing potential observations in different regions

of the tail. The exact same trajectories are chosen for both species. It should be noted that selecting a trajectory through a different part of the tail can be equivalent to a change in the upstream geometry, i.e., it does not matter if we change the orientation of Titan’s tail or the trajectory.

For a corotational flow, we do not see a clear split signature in the ion densities along the T9 trajectory (Fig. 9(c), which also shows the T9 CAPS ion data); instead, a broad profile with two small spikes for the heavy species and four spikes for the light species is observed. However there are no significant gaps in-between those spikes, except in the profile for the light species at 19:20. As can be seen in Fig. 9(a) and (b), it is easily possible to find spacecraft trajectories that show split features of varying sharpness, as well as trajectories that show only a single tail crossing. Looking at the densities plotted in red (trajectory located far downstream and south of the equatorial plane) both species show a double-peak, while in between the two peaks the densities fall below  $0.001 \text{ cm}^{-3}$  (less than 1% of the background density in our simulation). Compared to the CAPS measurements as indicated in Fig. 9(c), this trajectory would therefore have the density gap between the two spikes at roughly the observed location. For the densities plotted in blue (trajectory located north of the equatorial plane and closer to Titan) the light species  $L^+$  shows a triple peak structure and no longer drops to zero, which corresponds to the filaments seen in Fig. 8(d) and (g), while the heavy species shows no split feature. The black and green lines correspond to trajectories that are located even closer to Titan and slightly north of (black line) or in the moon’s equatorial plane (green line). Neither the light nor the heavy species show a split tail along these trajectories.

As is shown in Fig. 9, depending on the location of the spacecraft in Titan’s tail, there are indeed trajectories which show the split tail feature in the densities of one or more species, although for the T9 trajectory itself we do not see a clear split signature. The upstream flow parameters and the location of the dayside ionosphere with respect to the incident flow direction influences the position and densities of the filament structures. Asymmetries or fluctuations in the upstream flow parameters can therefore further enhance or displace the filaments. Based on our simulation results, the T9 observations can be qualitatively explained by Cassini first penetrating the Saturn-facing (dense) filament, which we see in all ionospheric species, and subsequently passing through the outer

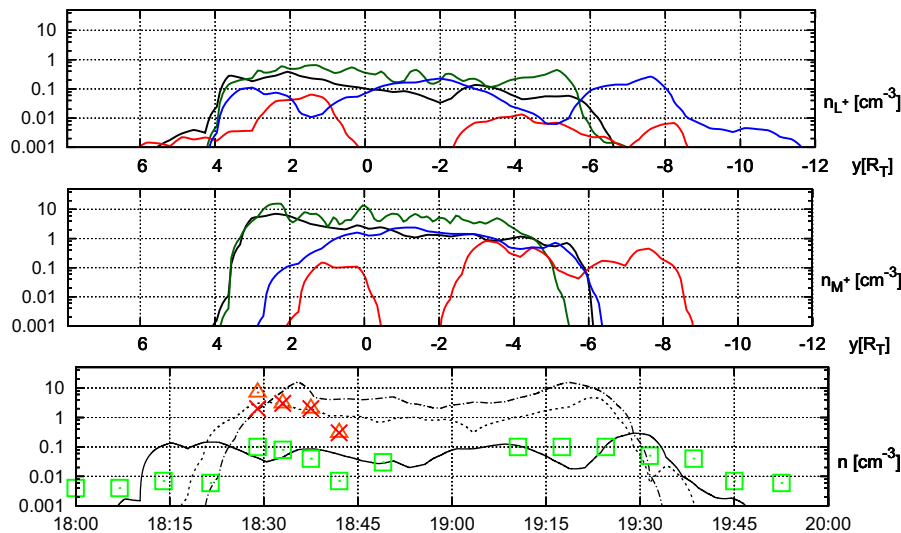


**Fig. 9.** Densities of the (a)  $L^+$  and (b)  $M^+$  species in the T9 run for different trajectories which are parallel to the  $y$ -axis. Black:  $x=4 R_T$ ,  $z=-2 R_T$ ; green:  $x=2 R_T$ ,  $z=0$ ; red:  $x=8 R_T$ ,  $z=-4 R_T$ ; and blue:  $x=6 R_T$ ,  $z=2 R_T$ . (c) Densities of the  $L^+$  (solid),  $M^+$  (dashed),  $H1^+$  (dot-dashed) species along the T9 trajectory. Also shown are the measured CAPS ion densities: green  $m/q=2$ , red:  $m/q=16$ , and orange:  $m/q=28$  (cf. Coates et al., 2012). (For interpretation of the references to color in this figure caption, the reader is referred to the web version of this paper.)

Saturn-averted filament of the light species. This would explain the observed composition (first interval both heavy and light ions, second interval only light ions, cf. Figure 2 of Coates et al., 2012) in the split signatures during the T9 encounter. It also explains why the measured densities were higher during the first event (on the Saturn-facing side), compared to the second event. This is because of the much higher ion production rate for the heavy species compared to the light species and the fact that the dayside ionosphere was located mainly on the Saturn-facing side as well.

### 3.3. Run #3: T63-type upstream conditions

During the T63 encounter, the background magnetic field was highly variable, possessing a north-south component with superimposed perturbations in the  $B_y$  component due to strong north-south oscillations of Saturn's magnetodisk current sheet (see Figure 2 of Simon et al., 2014). The average magnetic background vector we find from this data set mainly pointed in the north-south direction ( $\underline{B}_0 = (0.05, -0.33, -4.48)$ ), because the  $B_y$  oscillations cancel out during the time-averaging process (averaging interval of 2 h, each before and after Cassini entered the Titan interaction region). The upstream flow  $\underline{u}_0$  pointed in the corotational direction during this flyby (Coates et al., 2012). Since we chose the same upstream flow composition as in Run #1 (Voyager scenario, Table 3), the resulting upstream geometry is nearly identical compared to the previously discussed Voyager scenario (Section 3.1). The local time of the T63 encounter was at 17:00, so that the dayside ionosphere is approximately on the ramside of the moon (similar to Run #1, where the local time was 18:00). The results for the T63 encounter are therefore very similar as those for the Voyager scenario. However this is only because of the rough north-south approximation for the magnetic field, that does not take into account the high level of ambient magnetospheric variability.

Compared to T9, the trajectory of Cassini during T63 (see Fig. 1) was much closer ( $C/A$  at altitude  $1.9 R_T$ ) to Titan. Instead of taking place in the equatorial  $z=0$  plane, the trajectory was displaced by  $\sim 1.5 R_T$  in the positive  $z$  direction. Looking at the plots from the Voyager case, cf. Figs. 2(d)–(f) and 3(d)–(f), we expect to intersect parts of the cone structure that are related to the transport of ions from the ramside to the wakeside. The geometry of T63 is also suitable to probe asymmetries between the Saturn-facing and the Saturn-averted hemispheres due to the large gyroradii, since the flyby is located in a plane perpendicular to the magnetic field in our simulation.

These structures are indeed seen in Fig. 10, where the ionospheric densities from our T63 simulation in the  $z=1.5 R_T$  plane are plotted. The spacecraft trajectory is shown as well, with indications of the

intervals where the split signatures have been measured according to Coates et al. (2012) (also see Fig. 1 in this work). As we can see, located in the path of the spacecraft are at least two filaments (three for the  $L^+$  species) for all three species with a diameter of  $1.5\text{--}2 R_T$  and densities of  $\sim 10 \text{ cm}^{-3}$ . Note that the observations during T63 showed heavy (16 and 28 amu) and light (1–2 amu) ions in both events of the split signature, with densities  $< 10 \text{ cm}^{-3}$  (Coates et al., 2012), which is consistent with our results here. However, in our simulation the positions of the filaments do not coincide with the locations of the observations. This is likely because the stationary magnetic background field cannot represent the real magnetic fluctuations that were observed during T63.

The filaments on the Saturn-facing side of the tail in Fig. 10(a)–(c) are due to the transport of ions from the dense ionosphere on the ramside to the wakeside, the same as on the Saturn-averted side where the filaments are broadened due to the gyration of the ions in the  $y < 0$  half space. In between the filaments formed by  $M^+$  and  $H^+$  (see Fig. 10(b) and (c)) the density is decreased, i.e., we see a cut through the cone structure explained in Section 3.1, which is asymmetric in this plane (cf. Fig. 3(d)–(f)). The filament that can be seen at  $y = 1\text{--}2 R_T$  in Fig. 10(a) belongs to the outer filament structure of the light  $L^+$  species, which is also present in this slightly elevated plane ( $z = 1.5 R_T$ , cf. Fig. 2(g)).

In summary, the split tail detection during the T63 encounter is well explained with the picture of the tail structure established by this study, despite the large fluctuations of the ambient magnetospheric field. At T63, Cassini crossed through the cone behind Titan, which arises from the transport of ions from the ramside towards the wakeside. The outer filaments of the light species were probably not intersected during T63. However, we again note that our model does not consider the oscillatory motion of Saturn's magnetodisk during T63, which may very well have affected the locations of the individual tail filaments.

Fig. 10 (a)–(c) suggests that, under stationary upstream conditions, the positions of the modeled filaments could be brought into agreement with the observations by a rotation of the entire tail structure around the  $z$ -axis in a counterclockwise direction. Such a rotation may be caused, e.g., by a strong component of the incident flow velocity towards Saturn, or by fluctuations of the magnetic field as were observed during T63.

#### 3.3.1. T75 split signatures

The T75 trajectory is almost identical to the T9 trajectory (cf. Fig. 1), located far downstream ( $C/A$  at  $3.9 R_T$ ) in the equatorial plane ( $z=0$ ). The ambient magnetospheric field during the T75 encounter was heavily disturbed (even more so than during T63) by multiple crossings of Saturn's magnetospheric current sheet

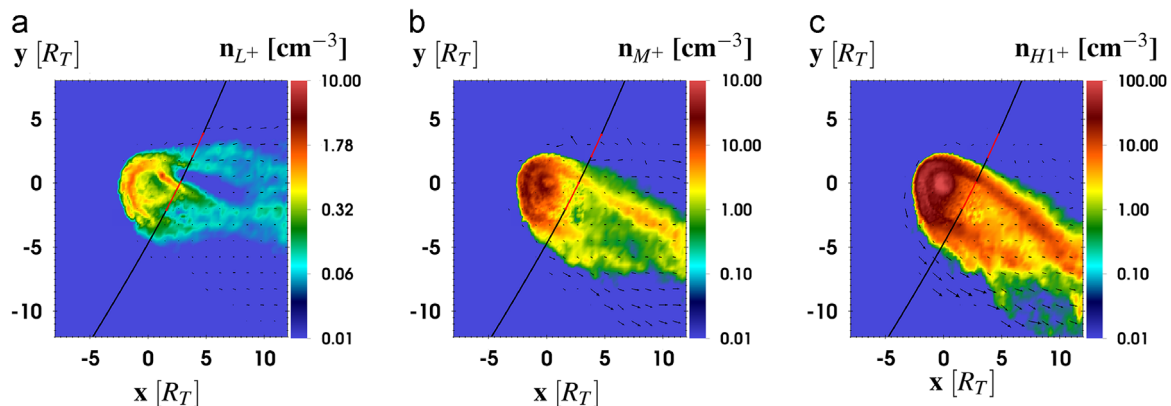


**Fig. 10.** Densities of the (a)  $L^+$ , (b)  $M^+$  and (c)  $H^+$  species in the  $z=1.5 R_T$  plane for T63. Arrows indicate velocities of the respective ion species. The black line shows the T63-trajectory, with the intervals of the observed split signatures marked in red. Cassini moved from  $y > 0$  towards  $y < 0$  during T63. (For interpretation of the references to color in this figure caption, the reader is referred to the web version of this paper.)

through Titan's orbital plane, near closest approach (cf. Figure 3 in Simon et al., 2014). Under these circumstances, a simulation of this encounter (using a stationary background magnetic field) is not very meaningful. However we have already shown that the filamentation off Titan's tail is a common feature. The fluctuations in the magnetic background field (corresponding to rotations of the tail structures) may even be beneficial for a split tail detection (see also Simon et al., 2014). The changes in the magnetic field can sweep a single filament back and forth over the spacecraft's trajectory, making Cassini detect the same structure twice or rotate additional filaments into the plane of the spacecraft trajectory.

#### 4. Summary

In this study, we applied a hybrid model of Titan's plasma interaction to obtain an understanding of the split signatures which were detected in Titan's tail during the T9, T63 and T75 encounters. Our major findings are as follows:

- Spatial inhomogeneities and filamentation of Titan's tail, which allow the detection of split signatures along an appropriate flyby trajectory, are a common feature of the moon's plasma interaction. The filamentation is most pronounced in a plane through the center of Titan which is perpendicular to the magnetic field as well as in a plane that contains the center of Titan and  $\underline{B}_0$  and  $\underline{u}_0$ .
- The collisional deceleration of the plasma, the strong density gradients near Titan and the deflection of ions from the ramside around Titan are mainly responsible for the observed filament structures. Ions of all species are accelerated radially away from Titan due to the pressure gradient force and then escape along trajectories aligned with the draped magnetic field. Similar to cometary plasma interactions, the pressure gradient force leads to an increased size of the obstacle to the incident plasma flow, which allows the filaments to separate from each other and to form the cone structure as well as the outer filaments of the light species.
- Light ions (1,2 amu) escape along draped field lines into the magnetic lobes and form the outer filaments of the split tail that have a crescent shape in the plane perpendicular to  $\underline{u}_0$ . These filaments are most pronounced in a plane through the center of Titan, containing  $\underline{u}_0$  and  $\underline{B}_0$  (i.e., the plane whose normal vector is  $\underline{E}_0$ ). In the direction of the convective electric field, these filaments are much less prominent.
- Transport of ions from the ramside to the wakeside produces a cone structure behind Titan: at the surface of the cone the ions are clustered into filaments with a thickness of 1–2  $R_T$ , and inside of the cone the density is reduced. The cone's apex denotes the point where these filaments merge into a single plasma tail. This effect is seen for all ionospheric species. In the plane perpendicular to the magnetic field, this structure is asymmetric towards the direction of  $\underline{E}_0 = -\underline{u}_0 \times \underline{B}_0$ , where it frays out due to the cycloidal motion of the pick-up ions.
- The locations and densities of the filaments strongly depend on the upstream flow parameters and the orientation of the day-side ionosphere with respect to the incident flow. They are easy to miss by Cassini.
- The T9 observations can be qualitatively explained by a crossing of Cassini through the Saturn-facing filament of the cone structure in the first event, and a subsequent crossing through the Saturn-averted outer filament of the light species in the second event. The upstream magnetic field orientation during T9 was beneficial for the detection of these filaments (flyby plane nearly coincident with the  $\underline{u}_0 \times \underline{B}_0$  plane, where the outer filaments of the light species are most pronounced).
- The T63 observations are consistent with a crossing of Cassini through the cone region. The detection of heavy ions in both events of the split signature supports this further. For T75, a double-detection of the same tail filament is a possible explanation, due to rotations of the tail by the large fluctuations in the ambient magnetic field. Likewise, it is possible that those fluctuations simply rotated two separate filaments into the spacecraft trajectory.

Although the Cassini Plasma Spectrometer ceased to operate in mid 2012 (Smith and Rymer, 2014), future studies of possible split signatures in Titan's tail can be performed by using electron and ion data from the RWPS and INMS instruments. These instruments have been used successfully in the past to identify interesting features of electrons and outflowing ions in Titan's upper ionosphere and the tail region (e.g., Edberg et al., 2010; Westlake et al., 2012). Our future work will also focus on the search for similar split-tail structures at other non-magnetized Solar system bodies (Venus, Mars, and comets).

#### Acknowledgements

The work of Moritz Feyerabend and Sven Simon was financially supported by the Deutsche Forschungsgemeinschaft (DFG) under Grant SI1753/1-1. The authors thank Joachim Saur for careful inspection of the paper and for valuable comments.

#### References

- Arridge, C.S., André, N., Bertucci, C.L., Garnier, P., Jackman, C.M., Németh, Z., Rymer, A.M., Sergis, N., Szego, K., Coates, A.J., Crary, F.J., 2011. Upstream of Saturn and Titan. *Space Sci. Rev.* 162 (1–4), 25–83.
- Bagdonat, T., 2005. Hybrid Simulation of Weak Comets (Ph.D. thesis). Technische Universität Braunschweig.
- Bertucci, C., Achilleos, N., Dougherty, M.K., Modolo, R., Coates, A.J., Szego, K., Masters, A., Ma, Y., Neubauer, F.M., Garnier, P., Wahlund, J.-E., Young, D.T., 2008. The magnetic memory of Titan's ionized atmosphere. *Science* 321 (5895), 1475–1478. <http://dx.doi.org/10.1126/science.1159780>.
- Bertucci, C., Duru, F., Edberg, N., Fraenz, M., Martinecz, C., Szego, K., Vaisberg, O., 2011. The induced magnetospheres of Mars, Venus, and Titan. *Space Sci. Rev.* 162 (December), 113–171.
- Bertucci, C., Hamilton, D.C., Kurth, W.S., Hospodarsky, G., Mitchell, D., Sergis, N., Edberg, N.J.T., Dougherty, M.K., 2015. Titan's interaction with the supersonic solar wind. *Geophys. Res. Lett.* 42 (January), 193–200.
- Bertucci, C., Neubauer, F.M., Szego, K., Wahlund, J.-E., Coates, A.J., Dougherty, M.K., Young, D.T., Kurth, W.S., 2007. Structure of Titan's mid-range magnetic tail: Cassini magnetometer observations during the T9 flyby. *Geophys. Res. Lett.* 34 (November (24)), L24S02.
- Bertucci, C., Sinclair, B., Achilleos, N., Hunt, P., Dougherty, M.K., Arridge, C.S., 2009. The variability of Titan's magnetic environment. *Planet. Space Sci.* 57 (14–15), 1813–1820.
- Böswetter, A., Bagdonat, T., Motschmann, U., Sauer, K., 2004. Plasma boundaries at Mars: a 3-D simulation study. *Ann. Geophys.* 22 (December), 4363–4379.
- Coates, A.J., Crary, F.J., Lewis, G.R., Young, D.T., Waite, J.H., Sittler, E.C., 2007a. Discovery of heavy negative ions in Titan's ionosphere. *Geophys. Res. Lett.* 34 (November (24)), L24S02.
- Coates, A.J., Crary, F.J., Young, D.T., Szego, K., Arridge, C.S., Bebesi, Z., Sittler, E.C., Hartle, R.E., Hill, T.W., 2007b. Ionospheric electrons in Titan's tail: plasma structure during the Cassini T9 encounter. *Geophys. Res. Lett.* 34 (24), L24S05.
- Coates, A.J., Wahlund, J.-E., Ågren, K., Edberg, N., Cui, J., Wellbrock, A., Szego, K., 2011. Recent results from Titan's ionosphere. *Space Sci. Rev.* 162 (December), 85–111.
- Coates, A.J., Wellbrock, A., Lewis, G.R., Arridge, C.S., Crary, F.J., Young, D.T., Thomsen, M.F., Reisenfeld, D.B., Sittler Jr., E.C., Johnson, R.E., Szego, K., Bebesi, Z., Jones, G. H., 2012. Cassini in Titan's tail: CAPS observations of plasma escape. *J. Geophys. Res. (Space Phys.)* 117, A05324.
- Cravens, T.E., Robertson, I.P., Waite, J.H., Yelle, R.V., Kasprzak, W.T., Keller, C.N., Ledvina, S.A., Niemann, H.B., Luhmann, J.G., McNutt, R.L., Ip, W.-H., De La Haye, V., Mueller-Wodarg, I., Wahlund, J.-E., Anicich, V.G., Vuitton, V., 2006. Composition of Titan's ionosphere. *Geophys. Res. Lett.* 33 (1–4), L07105. <http://dx.doi.org/10.1029/2005GL025575>.
- Cui, J., Yelle, R., Vuitton, V., Waite, J.H., Kasprzak, W., Gell, D., Niemann, H., Müller-Wodarg, I., Borggren, N., Fletcher, G., Patrick, E., Raean, E., Magee, B., 2009.

- Analysis of Titan's neutral upper atmosphere from Cassini ion neutral mass spectrometer measurements. *Icarus* 200(2), 581–615.
- Edberg, N.J.T., Wahlund, J.-E., Ågren, K., Morooka, M.W., Modolo, R., Bertucci, C., Dougherty, M.K., 2010. Electron density and temperature measurements in the cold plasma environment of Titan: implications for atmospheric escape. *Geophys. Res. Lett.* 37 (October), 20105.
- Galand, M., Coates, A.J., Cravens, T.E., Wahlund, J.-E., 2014. Titan's ionosphere. In: Müller-Wodarg, I., Griffith, C.A., Lellouch, E., Cravens, T.E. (Eds.), *Titan: Interior, Surface, Atmosphere, and Space Environment*. Cambridge University Press, Cambridge, UK, p. 376f.
- Kallio, E., Sillanpää, I., Jarvinen, R., Janhunen, P., Dougherty, M., Bertucci, C., Neubauer, F., 2007. Morphology of the magnetic field near Titan: hybrid model study of the Cassini T9 flyby. *Geophys. Res. Lett.* 34 (October (24)), L24S09.
- Krasnopolsky, V.A., 2009. A photochemical model of Titan's atmosphere and ionosphere. *Icarus* 201 (1), 226–256.
- Kriegel, H., 2014. *The Plasma Environments of Saturn's Moons Enceladus and Rhea: Modeling of Cassini Magnetic Field Data* (Ph.D. thesis). Technische Universität Braunschweig.
- Kriegel, H., Simon, S., Meier, P., Motschmann, U., Saur, J., Wennmacher, A., Strobel, D.F., Dougherty, M.K., 2014. Ion densities and magnetic signatures of dust pickup at Enceladus. *J. Geophys. Res. (Space Phys.)* 119 (4), 2740–2774.
- Kriegel, H., Simon, S., Motschmann, U., Saur, J., Neubauer, F.M., Persoon, A.M., Dougherty, M.K., Gurnett, D.A., 2011. Influence of negatively charged plume grains on the structure of Enceladus' Alfvén wings: hybrid simulations versus Cassini MAG data. *J. Geophys. Res.* 116 (A10), A10223.
- Krupp, N., Roussos, E., Kriegel, H., Kollmann, P., Kivelson, M.G., Kotova, A., Paranicas, C., Mitchell, D.G., Krimigis, S.M., Khurana, K.K., 2013. Energetic particle measurements in the vicinity of Dione during the three Cassini encounters 2005–2011. *Icarus* 226 (September), 617–628.
- Ledvina, S.A., Brecht, S.H., Cravens, T.E., 2012. The orientation of Titan's dayside ionosphere and its effects on Titan's plasma interaction. *Earth Planets Space* 64 (2), 207–230.
- Lipatov Jr., A.S., Sittler, E.C., Hartle, R., Cooper, J., Simpson, D., 2012. Saturn's magnetosphere interaction with titan for (T9) encounter: 3d hybrid modeling and comparison with {CAPS} observations. *Planet. Space Sci.* 61(1), 66–78.
- Ma, Y.-J., Nagy, A.F., Cravens, T.E., Sokolov, I.V., Clark, J., Hansen, K.C., 2004. 3-D global MHD prediction for the first close flyby of Titan by Cassini. *Geophys. Res. Lett.* 31 (L22803), 1–4.
- Ma, Y.-J., Nagy, A.F., Cravens, T.E., Sokolov, I.V., Hansen, K.C., Wahlund, J.-E., Cray, F. J., Coates, A.J., Dougherty, M.K., 2006. Comparisons between MHD model calculations and observations of Cassini flybys of Titan. *J. Geophys. Res.* 111, A05207.
- Ma, Y.-J., Nagy, A.F., Toth, G., Cravens, T.E., Russell, C.T., Gombosi, T.I., Wahlund, J.-E., Cray, F.J., Coates, A.J., Bertucci, C.L., Neubauer, F.M., 2007. 3D global multi-species Hall-MHD simulation of the Cassini T9 flyby. *Geophys. Res. Lett.* 34 (December), L24S10.
- Modolo, R., Chanteur, G.M., Wahlund, J.-E., Canu, P., Kurth, W.S., Gurnett, D., Matthews, A.P., Bertucci, C., 2007a. Plasma environment in the wake of Titan from hybrid simulation: a case study. *Geophys. Res. Lett.* 34. <http://dx.doi.org/10.1029/2007GL030489>.
- Modolo, R., Wahlund, J.-E., Boström, R., Canu, P., Kurth, W.S., Gurnett, D., Lewis, G.R., Coates, A.J., 2007b. Far plasma wake of Titan from the RPWS observations: a case study. *Geophys. Res. Lett.* 34, L24S04. <http://dx.doi.org/10.1029/2007GL030482>.
- Müller, J., Simon, S., Motschmann, U., Glassmeier, K.H., Saur, J., Schuele, J., Pringle, G. J., 2010. Magnetic field fossilization and tail reconfiguration in Titan's plasma environment during a magnetopause passage: 3D adaptive hybrid code simulations. *Planet. Space Sci.* 58 (12), 1526–1546. <http://dx.doi.org/10.1016/j.pss.2010.07.018>.
- Müller, J., Simon, S., Motschmann, U., Schüle, J., Glassmeier, K., Pringle, G.J., 2011. A I.K.E.F.: adaptive hybrid model for space plasma simulations. *Comput. Phys. Commun.* 182 (4), 946–966. <http://dx.doi.org/10.1016/j.cpc.2010.12.033>.
- Neubauer, F.M., Backes, H., Dougherty, M.K., Wennmacher, A., Russell, C.T., Coates, A., Young, D., Achilleos, N., Andre, N., Arridge, C.S., Bertucci, C., Jones, G.H., Khurana, K.K., Knetter, T., Law, A., Lewis, G.R., Saur, J., 2006. Titan's near magnetotail from magnetic field and plasma observations and modelling: Cassini flybys TA, TB and T3. *J. Geophys. Res.* 111, A10220.
- Neubauer, F.M., Gurnett, D.A., Scudder, J.D., Hartle, R.E., 1984. Titan's magnetospheric interaction. In: Gehrels, T., Matthews, M.S. (Eds.), *Saturn*. University of Arizona Press, Tucson, Arizona, pp. 760–787.
- Richards, P.G., Fennelly, J.A., Torr, D.G., 1994. EUVAC: a solar EUV flux model for aeronomic calculations. *J. Geophys. Res.* 99 (May), 8981–8992.
- Roussos, E., Mueller, J., Simon, S., Boeswetter, A., Motschmann, U., Krupp, N., Fraenz, M., Woch, J., Khurana, K.K., Dougherty, M.K., 2008. Plasma and fields in the wake of Rhea: 3-D hybrid simulation and comparison with Cassini data. *Ann. Geophys.* 26 (3), 619–637.
- Schunk, R., Nagy, A., 2009. *Ionospheres*, 2nd ed. Cambridge University Press, Cambridge, UK.
- Simon, S., 2009. Real-time 3D hybrid simulation of Titan's plasma interaction during a solar wind excursion. *Ann. Geophys.* 27 (9), 3349–3365.
- Simon, S., Boeswetter, A., Bagdonat, T., Motschmann, U., 2007a. Physics of the ion composition boundary: a comparative 3D hybrid simulation study of Mars and Titan. *Ann. Geophys.* 25 (1), 99–115.
- Simon, S., Boeswetter, A., Bagdonat, T., Motschmann, U., Glassmeier, K.-H., 2006. Plasma environment of Titan: a 3-d hybrid simulation study. *Ann. Geophys.* 24 (3), 1113–1135.
- Simon, S., Boeswetter, A., Bagdonat, T., Motschmann, U., Schuele, J., 2007b. Three-dimensional multispecies hybrid simulation of Titan's highly variable plasma environment. *Ann. Geophys.* 25 (1), 117–144.
- Simon, S., Kleindienst, G., Boeswetter, A., Bagdonat, T., Motschmann, U., Glassmeier, K.-H., Schuele, J., Bertucci, C., Dougherty, M.K., 2007c. Hybrid simulation of Titan's magnetic field signature during the Cassini T9 flyby. *Geophys. Res. Lett.* 34 (L24S08).
- Simon, S., Kriegel, H., Saur, J., Wennmacher, A., Neubauer, F.M., Roussos, E., Motschmann, U., Dougherty, M.K., 2012. Analysis of Cassini magnetic field observations over the poles of Rhea. *J. Geophys. Res. (Space Phys.)* 117 (July), 7211.
- Simon, S., Motschmann, U., 2009. Titan's induced magnetosphere under non-ideal upstream conditions: 3D multi-species hybrid simulations. *Planet. Space Sci.* 57 (14–15), 2001–2015. <http://dx.doi.org/10.1016/j.pss.2009.08.010>.
- Simon, S., Motschmann, U., Kleindienst, G., Saur, J., Bertucci, C., Dougherty, M., Arridge, C., Coates, A., 2009a. Titan's plasma environment during a magnetosheath excursion: real-time scenarios for Cassini's T32 flyby from a hybrid simulation. *Ann. Geophys.* 27 (2), 669–685.
- Simon, S., Neubauer, F.M., Wennmacher, A., Dougherty, M.K., 2014. Variability of Titan's induced magnetotail: Cassini magnetometer observations. *J. Geophys. Res. (Space Phys.)* 119 (3), 2024–2037.
- Simon, S., Saur, J., Neubauer, F., Motschmann, U., Dougherty, M., 2009b. Plasma wake of Tethys: hybrid simulations versus Cassini MAG data. *Geophys. Res. Lett.* 36 (4), L04108.
- Simon, S., Treeck, S.C., Wennmacher, A., Saur, J., Neubauer, F.M., Bertucci, C.L., Dougherty, M.K., 2013. Structure of Titan's induced magnetosphere under varying background magnetic field conditions: survey of Cassini magnetometer data from flybys TA-T85. *J. Geophys. Res. (Space Phys.)* 118 (4), 1679–1699.
- Simon, S., Wennmacher, A., Neubauer, F., Bertucci, C., Kriegel, H., Saur, J., Russell, C., Dougherty, M., 2010. Titan's highly dynamic magnetic environment: a systematic survey of Cassini magnetometer observations from flybys TA–T62. *Planet. Space Sci.* 58 (10), 1230–1251. <http://dx.doi.org/10.1016/j.pss.2010.04.021>.
- Sittler, E.C., Hartle, R.E., Johnson, R.E., Cooper, J.F., Lipatov, A.S., Bertucci, C., Coates, A.J., Szego, K., Shappirio, M., Simpson, D.G., Wahlund, J.-E., 2010. Saturn's magnetospheric interaction with Titan as defined by Cassini encounters T9 and T18: new results. *Planet. Space Sci.* 58 (3), 327–350.
- Smith, H.T., Rymer, A.M., 2014. An empirical model for the plasma environment along Titan's orbit based on Cassini plasma observations. *J. Geophys. Res.* 119 (7), 5674–5684.
- Szego, K., Bebesi, Z., Bertucci, C., Coates, A.J., Cray, F., Erdos, G., Hartle, R., Sittler, E. C., Young, D.T., 2007. Charged particle environment of Titan during the T9 flyby. *Geophys. Res. Lett.* 34 (24), L24S03.
- Vuitton, V., Duituit, O., Smith, M.A., Balucani, N., 2014. Chemistry of Titan's atmosphere. In: Müller-Wodarg, I., Griffith, C.A., Lellouch, E., Cravens, T.E. (Eds.), *Titan: Interior, Surface, Atmosphere, and Space Environment*. Cambridge University Press, Cambridge, UK, p. 224.
- Vuitton, V., Yelle, R.V., McEwan, M.J., 2007. Ion chemistry and N-containing molecules in Titan's upper atmosphere. *Icarus* 191 (November), 722–742.
- Wahlund, J.-E., Modolo, R., Bertucci, C., Coates, A.J., 2014. Titan's magnetospheric and plasma environment. In: Müller-Wodarg, I., Griffith, C.A., Lellouch, E., Cravens, T.E. (Eds.), *Titan: Interior, Surface, Atmosphere, and Space Environment*. Cambridge University Press, Cambridge, UK, p. 419.
- Westlake, J.H., Paranicas, C.P., Cravens, T.E., Luhmann, J.G., Mandt, K.E., Smith, H.T., Mitchell, D.G., Rymer, A.M., Perry, M.E., Waite Jr., J.H., Wahlund, J.-E., 2012. The observed composition of ions outflowing from Titan. *Geophys. Res. Lett.* 39 (October), 19104.